

AD-A216 436

ATTN FILE COPY

2



Defense Nuclear Agency
Alexandria, VA 22310-3398



DNA-TR-88-175

ACIRF User's Guide: Theory and Examples

R. A. Dana
Mission Research Corporation
P.O. Drawer 719
Santa Barbara, CA 93102-0719

December 1989

DTIC
ELECTE
DEC 27 1989
S D D
D G D

Technical Report

CONTRACT No. DNA 001-87-C-0169

Approved for public release;
distribution is unlimited.

89 12 26 120

Director
Defense Nuclear Agency
ATTN: TITL
Washington, DC 20305-1000

Director
Defense Nuclear Agency
ATTN: TITL
Washington, DC 20305-1000

DISTRIBUTION LIST UPDATE

This mailer is provided to enable DNA to maintain current distribution lists for reports. We would appreciate your providing the requested information.

- Add the individual listed to your distribution list.
- Delete the cited organization/individual.
- Change of address.

NAME: _____

ORGANIZATION: _____

OLD ADDRESS

CURRENT ADDRESS

TELEPHONE NUMBER: () _____

SUBJECT AREA(s) OF INTEREST:

DNA OR OTHER GOVERNMENT CONTRACT NUMBER: _____

CERTIFICATION OF NEED-TO-KNOW BY GOVERNMENT SPONSOR (if other than DNA).

SPONSORING ORGANIZATION: _____

CONTRACTING OFFICER OR REPRESENTATIVE: _____

SIGNATURE: _____

CUT HERE AND RETURN





CONVERSION TABLE

Conversion factors for U.S. Customary to metric (SI) units of measurement

MULTIPLY $\xrightarrow{\hspace{2cm}}$ BY $\xrightarrow{\hspace{2cm}}$ TO GET
 TO GET $\xleftarrow{\hspace{2cm}}$ BY $\xleftarrow{\hspace{2cm}}$ DIVIDE

angstrom	$1.000000 \times E -10$	meters (m)
atmosphere (normal)	$1.01325 \times E +2$	kilo pascal (kPa)
bar	$1.000000 \times E +2$	kilo pascal (kPa)
barn	$1.000000 \times E -28$	meter ² (m ²)
British thermal unit (thermochemical)	$1.054350 \times E +3$	joule (J)
calorie (thermochemical)	4.184000	joule (J)
cal (thermochemical) / cm ²	$4.184000 \times E -2$	mega joule/m ² (MJ/m ²)
curie	$3.700000 \times E +1$	*giga becquerel (GBq)
degree (angle)	$1.745329 \times E -2$	radian (rad)
degree Fahrenheit	$t_K = (t_F + 459.67)/1.8$	degree kelvin (K)
electron volt	$1.60219 \times E -19$	joule (J)
erg	$1.000000 \times E -7$	joule (J)
erg/second	$1.000000 \times E -7$	watt (W)
foot	$3.048000 \times E -1$	meter (m)
foot-pound-force	1.355818	joule (J)
gallon (U.S. liquid)	$3.785412 \times E -3$	meter ³ (m ³)
inch	$2.540000 \times E -2$	meter (m)
jerk	$1.000000 \times E +9$	joule (J)
joule/kilogram (J/kg) (radiation dose absorbed)	1.000000	Gray (Gy)
kilotons	4.183	terajoules
kip (1000 lbf)	$4.448222 \times E +3$	newton (N)
kip/inch ² (ksi)	$6.894757 \times E +3$	kilo pascal (kPa)
ktap	$1.000000 \times E +2$	newton-second/m ² (N-s/m ²)
micron	$1.000000 \times E -6$	meter (m)
mil	$2.540000 \times E -5$	meter (m)
mile (international)	$1.609344 \times E +3$	meter (m)
ounce	$2.834952 \times E -2$	kilogram (kg)
pound-force (lbs avoirdupois)	4.448222	newton (N)
pound-force inch	$1.129848 \times E -1$	newton-meter (N.m)
pound-force/inch	$1.751268 \times E +2$	newton/meter (N/m)
pound-force/foot ²	$4.788026 \times E -2$	kilo pascal (kPa)
pound-force/inch ² (psi)	6.894757	kilo pascal (kPa)
pound-mass (lbm avoirdupois)	$4.535924 \times E -1$	kilogram (kg)
pound-mass-foot ² (moment of inertia)	$4.214011 \times E -2$	kilogram-meter ² (kg.m ²)
pound-mass/foot ³	$1.601846 \times E +1$	kilogram/meter ³ (kg/m ³)
rad (radiation dose absorbed)	$1.000000 \times E -2$	**Gray (Gy)
roentgen	$2.579760 \times E -4$	coulomb/kilogram (C/kg)
shake	$1.000000 \times E -8$	second (s)
slug	$1.459390 \times E +1$	kilogram (kg)
torr (mm Hg, 0° C)	$1.333220 \times E -1$	kilo pascal (kPa)

*The becquerel (Bq) is the SI unit of radioactivity; 1 Bq = 1 event/s.

**The Gray (Gy) is the SI unit of absorbed radiation.

TABLE OF CONTENTS

Section	Page
CONVERSION TABLE	iii
LIST OF ILLUSTRATIONS	vi
LIST OF TABLES	vii
1 INTRODUCTION	1-1
2 THEORY	2-1
2.1 GENERALIZED POWER SPECTRAL DENSITY (GPSD).	2-1
2.1.1 Mutual Coherence Function.	2-1
2.1.2 Angular-Delay Power Spectral Density.	2-4
2.1.3 Doppler Spectra.	2-5
2.1.4 Frequency Selective Bandwidth and Angle of Arrival Variance.	2-7
2.1.5 Diffraction Limited Form of GPSD.	2-9
2.2 ANTENNA EFFECTS.	2-9
2.2.1 Antenna Coordinate System.	2-10
2.2.2 Antenna Beam Profile.	2-10
2.2.3 Antenna Filtering Equations.	2-13
2.2.4 Antenna Filtering Effects.	2-15
3 CHANNEL SIMULATION	3-1
3.1 FROZEN-IN MODEL.	3-2
3.1.1 Discrete Evaluation of the GPSD.	3-3

TABLE OF CONTENTS (CONCLUDED)

Section	Page
3.1.2 Random Realizations of the Impulse Response Function. . .	3-4
3.1.3 Grid Sizes.	3-6
3.2 TURBULENT MODEL.	3-9
4 EXAMPLES	4-1
4.1 MATCHED FILTER OUTPUT.	4-1
4.2 SCINTILLATION EFFECTS ON MATCHED FILTER OUTPUT.	4-3
4.2.1 Frequency Selective Effects.	4-3
4.2.2 Spatially Selective Effects.	4-5
5 LIST OF REFERENCES	5-1
 Appendices	
A INPUTS AND OUTPUTS OF ACIRF	A-1
A.1 ACIRF INPUT FILE.	A-1
A.2 FORMATTED ACIRF OUTPUT FILE.	A-1
A.3 UNFORMATTED ACIRF OUTPUT FILES.	A-9
B ACCURACY OF ANGULAR INTEGRATION TECHNIQUES	B-1
B.1 INTRODUCTION	B-1
B.2 ALGORITHMS	B-3
B.3 RESULTS	B-5



Accession For	
NTIS CRA&I	<input checked="" type="checkbox"/>
DTIC TAB	<input type="checkbox"/>
Unannounced	<input type="checkbox"/>
Justification _____	
By _____	
Distribution /	
Availability Codes	
Dist	Avail and/or Special
A-1	

LIST OF ILLUSTRATIONS

Figure		Page
2.1	Scattering coordinate system	2-4
2.2	Example of the generalized power spectral density	2-8
2.3	Antenna coordinate system	2-11
2.4	Generalized power spectra at the outputs of circular antennas .	2-16
2.5	Scattering loss for a uniformly weighted circular antenna	2-17
2.6	Filtered frequency selective bandwidth for a uniformly weighted circular antenna	2-19
2.7	Filtered decorrelation time for a uniformly weighted circular antenna	2-19
4.1	Effects of frequency selective fading	4-4
4.2	Comparison of matched filter output amplitude for the frozen-in and turbulent models	4-6
4.3	Effects of spatially selective fading	4-8
4.4	Effects of beam pointing	4-9
B.1	Relative error for pointing angle of 0	B-6
B.2	Relative error for pointing angle of $\theta_0/2$	B-6
B.3	Relative error for pointing angle of θ_0	B-7

LIST OF TABLES

Table		Page
A.1	Key ACIRF inputs	A-2
A.2	Example ACIRF input file	A-3
A.3a	Example ACIRF output file (page 1, summary of input and ensemble values)	A-4
A.3b	Example ACIRF output file (page 2, summary for antenna 1)	A-5
A.3c	Example ACIRF output file (page 3, summary for antenna 2)	A-6
A.3d	Example ACIRF output file (page 4, summary for antenna 3)	A-7
A.3e	Example ACIRF output file (page 7, ensemble and measured antenna output cross correlation coefficients)	A-8
A.4	Structure of unformatted ACIRF output files	A-10
A.5	Fortran code that generates character identification record . . .	A-10
A.6	Fortran code that generates floating point header records A and B	A-10
A.7	Description of header Record A	A-11
A.8	Listing of ACIRF subroutine WRITER	A-12
A.9	Listing of ACIRF subroutine READER	A-14

SECTION 1

INTRODUCTION

Design and evaluation of radio frequency systems that must operate through ionospheric disturbances resulting from high altitude nuclear detonations requires an accurate channel model. This model must include the effects of scintillation caused by the ionosphere and the effects of high gain antennas that may be used to receive the signals. Such a model can then be used to construct realizations of the received signal for use in digital simulations of trans-ionospheric links or for use in hardware channel simulators.

The propagation channel is conveniently represented in terms of the time-varying channel impulse response function $h(\tau, t)$ or, equivalently, by its Fourier transform, the time-varying channel transfer function $H(\omega, t)$. The former is the channel response at time t to an impulse applied at $t - \tau$. The latter is the channel response to a sinusoidal excitation at radian frequency ω . The received signal $u(t)$ is the convolution of the channel impulse response function and the transmitted modulation $m(t)$:

$$u(t) = \int_0^{\infty} h(\tau, t) m(t - \tau) d\tau \quad (1.1)$$

The purpose of this report is to describe the Fortran channel model ACIRF (Antenna/Channel Impulse Response Function) which generates random realizations of the impulse response function at the outputs of multiple antennas. The theory behind the impulse response function has been discussed by numerous authors (see, for example, Knepp 1982 or Dana 1986). The latter reference describes the theory of propagation through random media and antenna aperture effects applications, and is one of the references from which ACIRF was developed. The other reference is Wittwer and Dana (1989). Channel simulation techniques without antennas have been described by Wittwer (1980) and Knepp and Wittwer (1984). The former reference contains a listing of the original CIRF program developed by Dr. Leon A. Wittwer of the Defense Nuclear Agency. Simulation techniques have been extended to include antenna effects in Dana (1986) and Wittwer and Dana (1989). ACIRF is intended replace the CIRF code. Thus ACIRF contains the channel models in CIRF without antennas plus it has new channel models that include antenna aperture effects.

Section 2 of this report briefly outlines the theory behind ACIRF. The Generalized Power Spectral Density (GPSD) function, which describes the second order statistics of the channel impulse response function, is discussed. The antenna beam profile parameters (beamwidths and pointing angles) are defined, and the effects of the antenna on the received signal statistics are described. Channel simulation techniques used in ACIRF are presented in Section 3. Section 4 presents examples of the output of a matched filter which illustrate the effects of scintillation and antennas on the received signal. The inputs and outputs of the ACIRF Fortran code are discussed in Appendix A.

SECTION 2

THEORY

The starting point for channel modeling is the generalized power spectral density (GPSD). This function describes the second-order statistics of the signal incident on the face of an antenna. When scintillation is intense or fully developed, the first-order signal amplitude statistics are well described by the Rayleigh probability distribution, and the signal phase is uniformly distributed over a 2π radian interval. The strong scattering limit can also be obtained by applying the central limit theorem to the superposition of the many randomly scattered waves which comprise the received signal under these conditions. The in-phase (I) and quadrature-phase (Q) components of the signal are then independent, zero-mean Gaussian random variables with variances equal to one-half the total signal power. These conditions are both necessary and sufficient for Rayleigh amplitude statistics.

2.1 GENERALIZED POWER SPECTRAL DENSITY (GPSD).

The derivation of the GPSD starts with Maxwell's equations from which the parabolic wave equation is derived (see, for example, Dana 1986). A necessary condition for the parabolic wave equation to be valid is that the phase perturbation over a distance comparable to a wavelength be small compared to one radian. A sufficient condition is that the angular deviation of the wave relative to the principal propagation path be small compared to one radian. These conditions are generally satisfied whenever attenuation of the propagating wave is not significant.

2.1.1 Mutual Coherence Function.

The parabolic wave equation can be solved to give the received electric field for a specific distribution of the index of refraction. The difficulty is that the index of refraction is a random process. The parabolic wave equation is therefore used to derive an equation for the two-position, two-frequency, two-time mutual coherence function, Γ , of the received electric field E :

$$\Gamma(x, y, \omega, t) = \langle E(x_1, y_1, \omega_1, t_1) E^*(x_2, y_2, \omega_2, t_2) \rangle \quad (2.1)$$

where $x = x_1 - x_2$ and $y = y_1 - y_2$ are relative positions in the plane of the receiver, $\omega = \omega_1 - \omega_2$ is radian frequency difference, and $t = t_1 - t_2$ is time difference.

The solution of the differential equation for the mutual coherence function provides a description of the second-order statistics of the received signal. The time variation part of the mutual coherence function takes on different forms depending on the nature of the propagation medium. Two limiting models are of interest. The first limit is the "frozen-in" model wherein the striations in the ionosphere act as a cohesive structure that moves relative to the propagation path. The time variations of the received signal are then a straightforward mapping of the diffracted electric field as it drifts past the receiver antenna. Thus, in this frozen-in model there is a strong coupling between the spatial and temporal variations of the received signal. The second limiting model is a "turbulent" situation wherein striations move differently at different points along the propagation path, causing time variations of the diffracted electric field to become decorrelated at different points in the receiver plane. The turbulent model therefore decouples the spatial and temporal variations of the received field.

Wittwer (1989) has recently proposed a "general" model that falls between these two limiting models. This model is currently being incorporated into a new version of ACIRF and will be the subject of a future volume of the ACIRF User's Guide.

The mutual coherence function for the frozen-in model is

$$\Gamma(x, y, \omega, t) = \left[1 + \frac{i\Lambda\omega}{\omega_{coh}}\right]^{-1/2} \left[1 + \frac{i\Lambda(\ell_x/\ell_y)^2\omega}{\omega_{coh}}\right]^{-1/2} \exp\left[-\frac{\omega^2}{\alpha^2}\right] \times \quad (2.2)$$

$$\exp\left[\frac{-(x - \ell_x t/\tau_0)^2/\ell_x^2}{1 + i\Lambda\omega/\omega_{coh}}\right] \exp\left[\frac{-y^2/\ell_y^2}{1 + i\Lambda(\ell_x/\ell_y)^2\omega/\omega_{coh}}\right] \quad \text{(Frozen-In Model)}$$

The coupling between spatial and temporal variations for the frozen-in model is a result of the $x - \ell_x t/\tau_0$ term. For the turbulent model, the mutual coherence function is

$$\Gamma(x, y, \omega, t) = \Gamma_T(t) \left[1 + \frac{i\Lambda\omega}{\omega_{coh}}\right]^{-1/2} \left[1 + \frac{i\Lambda(\ell_x/\ell_y)^2\omega}{\omega_{coh}}\right]^{-1/2} \exp\left[-\frac{\omega^2}{\alpha^2}\right] \times \quad (2.3)$$

$$\exp\left[\frac{-x^2/\ell_x^2}{1 + i\Lambda\omega/\omega_{coh}}\right] \exp\left[\frac{-y^2/\ell_y^2}{1 + i\Lambda(\ell_x/\ell_y)^2\omega/\omega_{coh}}\right] \quad \text{(Turbulent Model)}$$

where $\Gamma_T(t)$ is the temporal coherence function which does not depend on either the spatial variables or frequency.

By examining these two forms for the mutual coherence function, it can be seen that the decorrelation distance ℓ_x is the 1/e point of $\Gamma(x, 0, 0, 0)$, and the decorrelation distance ℓ_y is the 1/e point of $\Gamma(0, y, 0, 0)$. The asymmetry factor Λ is a function of the two decorrelation distances:

$$\Lambda = \left[\frac{2}{1 + (\ell_x/\ell_y)^4} \right]^{1/2} . \quad (2.4)$$

The coordinate system of the scattering is defined by the line of sight direction \hat{z} and the geomagnetic field \vec{B} at the altitude in the ionosphere where the scattering occurs. The orientation of the \hat{x} axis,

$$\hat{x} = \frac{\vec{B} \times \hat{z}}{|\vec{B}| \sin \Phi} ,$$

is chosen such that $\ell_x \leq \ell_y$. This scattering coordinate system is shown in Figure 2.1. The penetration angle Φ is the angle between the line of sight direction and the magnetic field.

In general, both decorrelation distances should be part of the specification of the channel parameters. However, if only the minimum decorrelation distance ℓ_x (also referred to as ℓ_0 in the literature) is specified, then the ratio of the decorrelation distances ℓ_y/ℓ_x can be estimated from the formula:

$$\frac{\ell_y}{\ell_x} = \sqrt{\cos^2 \Phi + q^2 \sin^2 \Phi} \quad (2.5)$$

where q is the axial ratio which is equal to the ratio of the characteristic length of striations along the field lines to the characteristic thickness in a direction normal to the field lines. The standard value for q has been 15. However, recent research on the physics of striations indicates that q may be as large as 70 (Wittwer 1988).

The decorrelation time τ_0 is the 1/e point of $\Gamma(0, 0, 0, t)$ for the frozen-in model. In order to maintain a consistent definition of decorrelation time, it will also be required that $\Gamma_T(\tau_0)$ equal 1/e for the turbulent model.

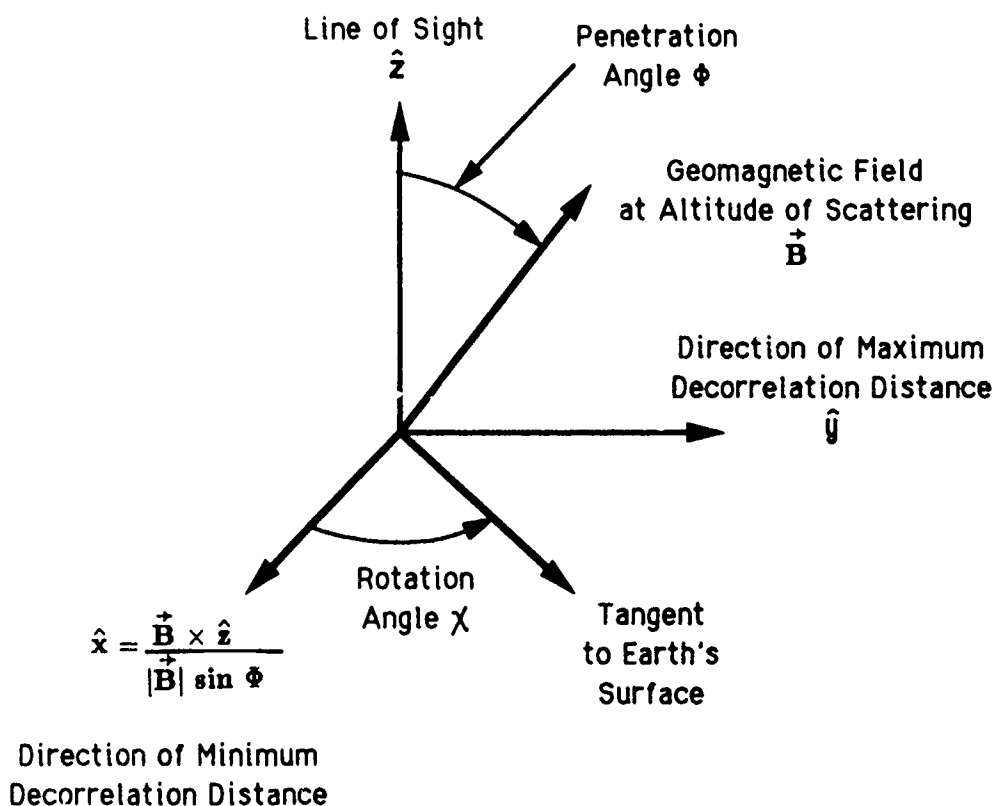


Figure 2.1. Scattering coordinate system.

The coherence bandwidth, ω_{coh} , is defined using the GPSD which will be discussed next. The quantity α is a delay parameter which is equal to the ratio of the time delay spread caused by diffraction to that caused by refraction. In strong scattering where diffractive effects dominate, the value of α is fairly large.

2.1.2 Angular-Delay Power Spectral Density.

The Fourier transform of the mutual coherence function is the generalized power spectral density of the received signal:

$$S(K_x, K_y, \tau, \omega_D) = \int_{-\infty}^{\infty} dx \int_{-\infty}^{\infty} dy \int_{-\infty}^{\infty} \frac{d\omega}{2\pi} \int_{-\infty}^{\infty} dt \Gamma(x, y, \omega, t) \times \exp[-i(K_x x + K_y y - \omega\tau + \omega_D t)] \quad (2.6)$$

where ω_D is the Doppler radian frequency, τ is the time delay, and K_x and K_y are related to the scattering angles θ_x and θ_y about the x and y axes as follows:

$$\begin{aligned} K_x &= \frac{2\pi \sin \theta_x}{\lambda} \\ K_y &= \frac{2\pi \sin \theta_y}{\lambda} \end{aligned} \quad (2.7)$$

The quantity $S(K_x, K_y, \tau, \omega_D) dK_x dK_y d\tau d\omega_D$ is the mean signal energy incident on the face of a receiving antenna arriving from angles K_x to $K_x + dK_x$ and K_y to $K_y + dK_y$; with delays in the interval τ to $\tau + d\tau$, and with Doppler frequencies in the interval ω_D to $\omega_D + d\omega_D$.

In general, the GPSD can be written as a product of a Doppler term times an angular-delay term,

$$S(K_x, K_y, \tau, \omega_D) = S_D(\omega_D) S_{K\tau}(K_x, K_y, \tau) \quad , \quad (2.8)$$

where the angular-delay part of the GPSD is

$$\begin{aligned} S_{K\tau}(K_x, K_y, \tau) &= \left[\frac{\pi}{2} \right]^{1/2} \alpha \omega_{coh} \ell_x \ell_y \exp \left[-\frac{K_x^2 \ell_x^2 + K_y^2 \ell_y^2}{4} \right] \times \\ &\exp \left\{ -\frac{\alpha^2}{2} \left[\omega_{coh} \tau - \frac{\Lambda(K_x^2 + K_y^2) \ell_x^2}{4} \right]^2 \right\} \quad . \end{aligned} \quad (2.9)$$

2.1.3 Doppler Spectra.

The Doppler part of the GPSD has different forms for the frozen-in and turbulent models. For the frozen-in model, the drift velocity of striations is chosen to be along the x -direction in the receiver plane. The Doppler component of the GPSD is then

$$S_D(\omega_D) = 2\pi \delta(\omega_D \tau_0 - K_x \ell_x) \quad (2.10)$$

where $\delta(\cdot)$ is the Dirac delta function. This choice for the orientation of the drift velocity minimizes the value of τ_0 . The decorrelation time in the frozen-in model is the time required for the diffraction pattern to drift one decorrelation distance in the receiver plane.

Combining Equations 2.8 through 2.10 and integrating over angle and delay gives the Doppler spectrum for the frozen-in model:

$$\begin{aligned} S(\omega_D) &= \int_{-\infty}^{\infty} \frac{dK_x}{2\pi} \int_{-\infty}^{\infty} \frac{dK_y}{2\pi} \int_{-\infty}^{\infty} d\tau S_D(\omega_D) S_{K\tau}(K_x, K_y, \tau) \\ &= \sqrt{\pi}\tau_0 \exp\left[-\frac{\tau_0^2\omega_D^2}{4}\right] \quad \text{(Frozen-In Model)} \end{aligned} \quad (2.11)$$

The temporal coherence function for this case also has a Gaussian form:

$$\Gamma_T(t) = \int_{-\infty}^{\infty} \exp(i\omega_D t) S(\omega_D) \frac{d\omega_D}{2\pi} = \exp\left[-\frac{t^2}{\tau_0^2}\right] \quad (2.12)$$

For the turbulent mode', the Doppler component of the GPSD is a function only of the Doppler frequency. In this model there is no coupling between scattering angle and Doppler frequency or, equivalently, between position and time. The Doppler spectrum is therefore independent of delay so the temporal variations exhibit the same rate at all delays. A mathematically convenient form of the Doppler spectrum for the turbulent model is the so-called f^{-4} spectrum:

$$S(\omega_D) = \frac{4\tau_0}{a} \frac{1}{[1 + \tau_0^2\omega_D^2/a^2]^2} \quad \text{(Turbulent Model)} \quad (2.13)$$

where the parameter a ($a = 2.146193$) is determined by the condition that $\Gamma_T(\tau_0)$ equal $1/e$. The corresponding temporal coherence function then has the form:

$$\Gamma_T(t) = \left[1 + \frac{a|t|}{\tau_0}\right] \exp\left[-\frac{a|t|}{\tau_0}\right] \quad (2.14)$$

2.1.4 Frequency Selective Bandwidth and Angle of Arrival Variance.

An important measure of the effects of scintillation on the propagation of wide bandwidth signals is the frequency selective bandwidth. This quantity is defined as

$$f_0 = \frac{1}{2\pi\sigma_\tau} \quad (2.15)$$

where σ_τ is the standard deviation of the time delay jitter of the received signal:

$$\sigma_\tau^2 = \langle \tau^2 \rangle - \langle \tau \rangle^2 \quad . \quad (2.16)$$

The moments of delay are calculated using the angular-delay part of the GPSD,

$$\langle \tau^n \rangle = \int_{-\infty}^{\infty} \frac{dK_x}{2\pi} \int_{-\infty}^{\infty} \frac{dK_y}{2\pi} \int_{-\infty}^{\infty} d\tau \tau^n S_{K\tau}(K_x, K_y, \tau) \quad . \quad (2.17)$$

These equations then give the relationship between ω_{coh} and the frequency selective bandwidth f_0 :

$$\omega_{coh} = 2\pi f_0 \sqrt{1 + 1/\alpha^2} \quad . \quad (2.18)$$

An important signal parameter for systems that utilize large aperture receiving antennas is the angular scattering variance. Whenever the striations in the ionosphere are not aligned with the propagation direction, which is typically the case, the angular scattering will be different about the x and y axes. The standard deviations of the angle of arrival fluctuations about the x and y axes are:

$$\begin{aligned} \sigma_{\theta_x} &= \frac{\lambda}{\sqrt{2\pi}\ell_x} \\ \sigma_{\theta_y} &= \frac{\lambda}{\sqrt{2\pi}\ell_y} \quad . \end{aligned} \quad (2.19)$$

If the propagation path is aligned with the striations in the ionosphere, the decorrelation distances in the x and y directions will be the same. In this isotropic case the scattering angles are the same in each direction. A three-dimensional plot of the isotropic one-dimensional GPSD is shown in Figure 2.2. This plot shows an example of the mean received power as a function of normalized angle-of-arrival, Kl_0 , and normalized time delay, $\omega_{coh}\tau$. For this isotropic case, the quantity K is either K_x or K_y since they are equal. Similarly, the quantity l_0 is either l_x or l_y . The value of α for this figure is taken to be 4, so consequently the quantity ω_{coh} is essentially equal to $2\pi f_0$. It can be seen from the figure that the power arriving at large angles is also the power arriving at long delays. The power arriving at long delays thus is more likely to be attenuated if the receiving antenna has a narrow beamwidth.

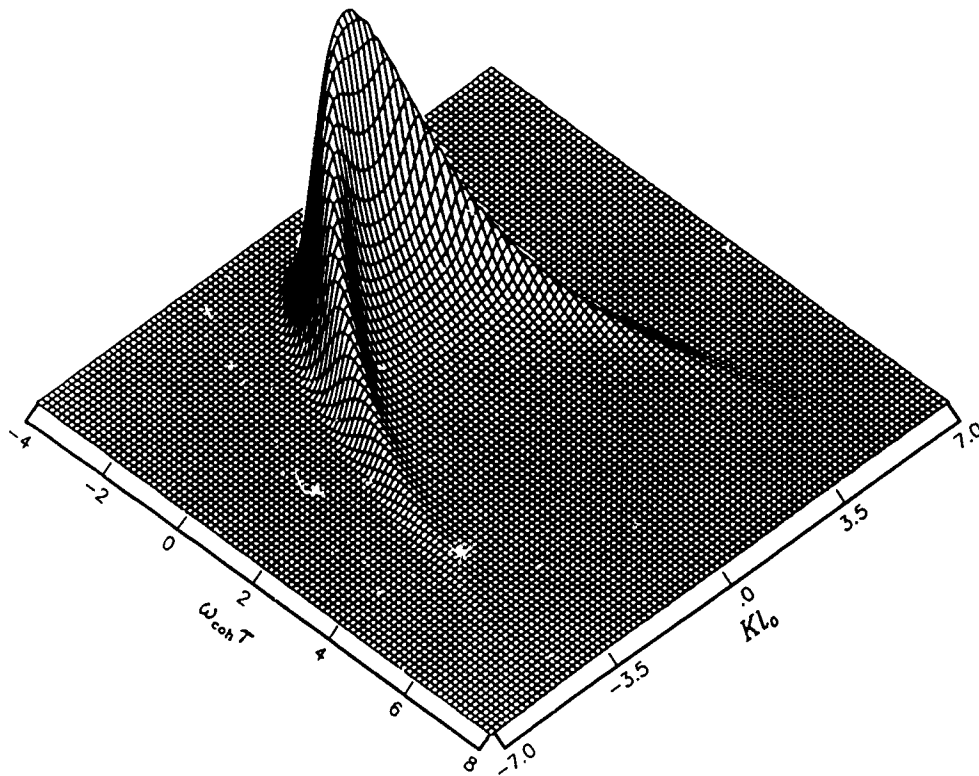


Figure 2.2. Example of the generalized power spectral density.

2.1.5 Diffraction Limited Form of GPSD.

Under the strong scattering conditions in the ionosphere that cause signal scintillation at radio frequencies, diffractive effects dominate refractive effects. In this case, the value of α in the GPSD is large. In the limit that α approaches infinity, the form of the GPSD can be simplified by noting that

$$\lim_{\alpha \rightarrow \infty} [\alpha \exp(-\alpha^2 x^2)] = \sqrt{\pi} \delta(x) \quad . \quad (2.20)$$

In this limit, the angular-delay part of the GPSD becomes

$$S_{K\tau}(K_x, K_y, \tau) = \pi \omega_{coh} \ell_x \ell_y \exp \left[-\frac{K_x^2 \ell_x^2 + K_y^2 \ell_y^2}{4} \right] \times \\ \delta \left[\omega_{coh} \tau - \frac{\Lambda(K_x^2 + K_y^2) \ell_x^2}{4} \right] \quad . \quad (2.21)$$

This geometric optics limit results in a delta function relationship between angle and delay. This form of the angular-delay part of the GPSD will be used to generate realizations of the impulse response function at the outputs of antennas.

2.2 ANTENNA EFFECTS.

The GPSD of the signal at the output of an antenna, $S_A(K, \tau, \omega_D)$, is given by (Frasier 1988)

$$S_A(K, \tau, \omega_D) = G(K - K_0) S(K, \tau, \omega_D) \quad (2.22)$$

where $G(K - K_0)$ is the two dimensional beam profile of an antenna pointing in the direction K_0 . The effect of the antenna then is to attenuate the received signal energy at angles outside of the main beam of the antenna. If the antenna is pointed along the line of sight, the signal energy that is attenuated by the antenna is that with large angles of arrival. This is also the energy with large times of arrival. The effect of the antenna will then be to reduce the received signal power, and also to reduce the delay spread of that energy.

2.2.1 Antenna Coordinate System.

The antenna coordinate system is shown in Figure 2.3. It is assumed that the face of the antenna is in the $x-y$ plane and the boresight is pointed along the line of sight. The beam in this figure is pointed away from the line of sight in the direction K_0 defined by a pointing angle ψ and an azimuth angle ϵ . The rotation angle is the angle between the scattering \hat{x} axis and an antenna axis \hat{u} . The antenna (\hat{u}, \hat{v}) coordinate system, where \hat{v} is in the $x-y$ plane and is orthogonal to \hat{u} , is chosen for convenience in describing the antenna beam profile. For example, if the antenna is rectangular, then the (\hat{u}, \hat{v}) axes should be aligned with the sides of the aperture. In this coordinate system, the antenna beam profile $G(\theta_u, \theta_v)$ is approximated as a product $G(\theta_u)$ times $G(\theta_v)$ where θ_u and θ_v are angles about the u and v axes respectively. In many cases, the axis \hat{u} will be parallel to the local earth tangent plane.

The components of the antenna pointing direction K_0 in terms of the rotation, pointing, and azimuth angles are

$$K_{0z} = \frac{2\pi}{\lambda} \sin \psi \cos(\chi + \epsilon) \quad (2.23)$$

$$K_{0y} = \frac{2\pi}{\lambda} \sin \psi \sin(\chi + \epsilon) \quad (2.24)$$

2.2.2 Antenna Beam Profile.

The antenna beam profile is assumed to have a Gaussian shape and to be separable in the $u-v$ coordinate system:

$$G(K_u, K_v) = \exp \left[-\alpha_u^2 K_u^2 - \alpha_v^2 K_v^2 \right] \quad (2.25)$$

The peak gain $G(0,0)$ has been set to unity because this value is usually included in the calculation of the mean received power. For either the u or the v direction, the antenna beam profile can also be written as

$$G(\theta) = \exp[-(\ln 2)(2\theta/\theta_0)^2] \quad (2.26)$$

where θ_0 is the 3 dB beamwidth [i.e. full width at half maximum, $G(\theta_0/2) = 1/2$]. Equating these two profiles gives

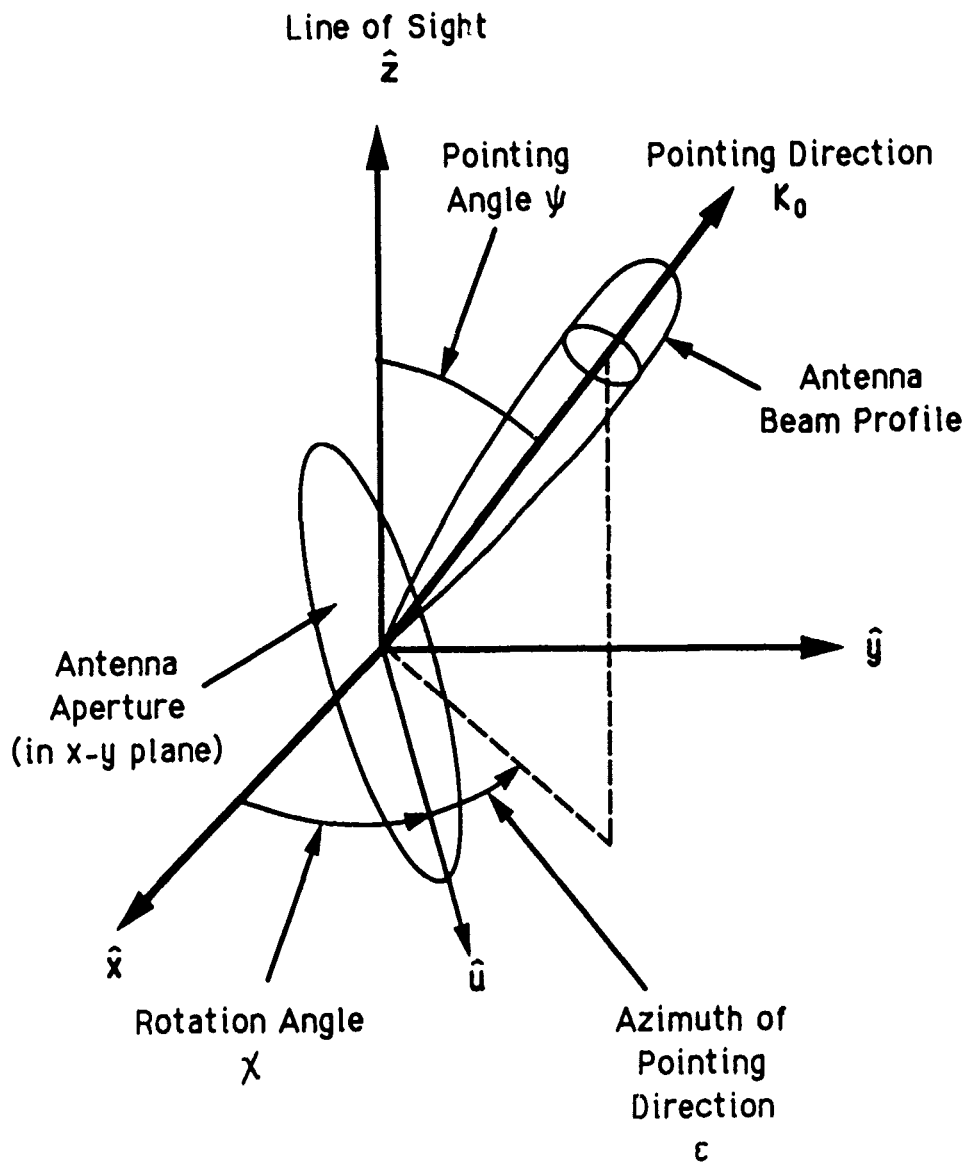


Figure 2.3. Antenna coordinate system.

$$\alpha_{\xi}^2 = \frac{(\ln 2)\lambda^2}{\pi^2 \theta_{0\xi}^2} \quad (2.27)$$

where $\theta_{0\xi}$ is the 3 dB beamwidth in the $\xi = u$ or the $\xi = v$ direction.

In the next subsections, the 3 dB beamwidths are related to antenna sizes for the special cases of uniformly weighted circular and rectangular apertures.

Uniformly Weighted Circular Apertures

For a uniformly weighted circular aperture, the well known form for the power beam profile is

$$G(\theta) = \frac{4J_1^2[\pi(D/\lambda) \sin \theta]}{[\pi(D/\lambda) \sin \theta]^2} \quad (2.28)$$

where $J_1(\cdot)$ is the Bessel function. The 3 dB full width at half maximum beamwidth, in terms of the diameter D , is

$$\theta_0 = 1.02899(\lambda/D) \text{ radians} \quad (2.29)$$

If this beam profile is approximated by a Gaussian profile with the same 3 dB beamwidth, then the coefficients that appear in Equation 2.24 are

$$\alpha_u^2 = \alpha_v^2 = \frac{(\ln 2)D^2}{(1.02899\pi)^2} \quad (2.30)$$

Uniformly Weighted Rectangular Apertures

For uniformly weighted rectangular apertures, the antenna beam profile in either the $\xi = u$ or $\xi = v$ direction has the familiar $\sin^2(x)/x^2$ form:

$$G_{\xi}(\theta_{\xi}) = \frac{\sin^2[\pi(D_{\xi}/\lambda) \sin \theta_{\xi}]}{[\pi(D_{\xi}/\lambda) \sin \theta_{\xi}]^2} \quad (2.31)$$

where D_{ξ} is the length of the aperture. The 3 dB beamwidth is

$$\theta_{0\xi} = 0.885893(\lambda/D_\xi) \text{ radians} \quad . \quad (2.32)$$

and the coefficients that appear in Equation 2.24 are

$$\alpha_\xi^2 = \frac{(\ln 2) D_\xi^2}{(0.885893\pi)^2} \quad . \quad (2.33)$$

2.2.3 Antenna Filtering Equations.

Frasier (1988) has derived filtering equations for an antenna pointing in an arbitrary direction away from the line of sight. The equations for the scattering loss, frequency selective bandwidth, decorrelation time and distances are reproduced here. Further details on the derivation of these equations may be found in Frasier (1988).

For an arbitrary antenna with a beam profile characterized by two beamwidths and for general anisotropic scattering, it is mathematically convenient to write the angular-delay part of the GPSD using matrix notation:

$$S_{K\tau}(\vec{K}, \tau) = \pi \omega_{coh} \ell_x \ell_y \exp[-\vec{K} \cdot \tilde{L} \cdot \vec{K}] \delta \left[\omega_{coh} \tau - \frac{\Lambda K^2 \ell_x^2}{4} \right] \quad (2.34)$$

where

$$K = \sqrt{K_x^2 + K_y^2} \quad (2.35)$$

is the magnitude of the vector \vec{K} , and the decorrelation length matrix \tilde{L} in the $x - y$ coordinate system is

$$\tilde{L} = \begin{bmatrix} \frac{\ell_x^2}{4} & 0 \\ 0 & \frac{\ell_y^2}{4} \end{bmatrix} \quad (2.36)$$

The mean received power at the output of the antenna, P_A , is

$$P_A = \left[\frac{\det(\tilde{L})}{\det(\tilde{Q})} \right]^{1/2} G(\vec{K}_0) \exp(\vec{m} \cdot \tilde{Q}^{-1} \cdot \vec{m}) \quad (2.37)$$

where $G(\vec{K}_0)$ is the line of sight gain of the antenna pointed in the direction \vec{K}_0 away from the line of sight,

$$\tilde{Q} = \tilde{L} + \tilde{\alpha} \quad (2.38)$$

$$\vec{m} = \tilde{\alpha} \cdot \vec{K}_0, \quad (2.39)$$

and where the matrix $\tilde{\alpha}$, in the $x - y$ coordinate system, is

$$\tilde{\alpha} = \begin{bmatrix} \alpha_u^2 \cos^2 \chi + \alpha_v^2 \sin^2 \chi & (\alpha_u^2 - \alpha_v^2) \sin \chi \cos \chi \\ (\alpha_u^2 - \alpha_v^2) \sin \chi \cos \chi & \alpha_u^2 \sin^2 \chi + \alpha_v^2 \cos^2 \chi \end{bmatrix}. \quad (2.40)$$

Note that Equation 2.36 is independent of the choice of coordinate systems as long as all of the matrices are expressed in the same coordinate system. The scattering loss, in decibels, of the antenna is just $-10 \log_{10}(P_A)$.

The antenna filtered values of the decorrelation distances are

$$\ell_{Az} = 2 \left[\frac{\det(\tilde{Q})}{Q_{yy}} \right]^{1/2} \quad (2.41)$$

$$\ell_{Ay} = 2 \left[\frac{\det(\tilde{Q})}{Q_{zz}} \right]^{1/2} \quad (2.42)$$

where Q_{zz} and Q_{yy} are the two diagonal components of \tilde{Q} in the $x - y$ coordinate system. Note that the filtered decorrelation distances depend only on the beamwidths of the antenna and are independent of pointing angle. However, as a beam is pointed away from the line of sight, the beamwidth will increase because of foreshortening of the aperture. Thus the independence of the antenna filtered decorrelation distances with pointing angle is only true for small pointing angles.

The antenna filtered decorrelation time for the frozen-in model, when the relative motion of the antenna and random diffraction pattern is in the x direction, is

$$\frac{\tau_A}{\tau_0} = \frac{\ell_{Ax}}{\ell_x} = \frac{2}{\ell_x} \left[\frac{\det(\tilde{Q})}{Q_{yy}} \right]^{1/2} \quad . \quad (\text{Frozen-in Model}) \quad (2.43)$$

The expression for τ_A/τ_0 is also independent of pointing angle. For the turbulent model,

$$\frac{\tau_A}{\tau_0} = 1 \quad . \quad (\text{Turbulent Model}) \quad (2.44)$$

Finally, the antenna filtered frequency selective bandwidth is

$$\frac{f_A}{f_0} = \frac{1}{\det(\tilde{L})} \left[\frac{\text{tr}(\tilde{L}^2)}{4\tilde{m} \cdot \tilde{Q}^{-3} \cdot \tilde{m} + \frac{\text{tr}(\tilde{Q}^2)}{\det^2(\tilde{Q})}} \right]^{1/2} \quad . \quad (2.45)$$

The form of this result emphasizes its invariance with respect to the choice of coordinate systems.

2.2.4 Antenna Filtering Effects.

The effect of antenna filtering is illustrated in Figure 2.4, which shows four plots of the GPSD at the outputs of four uniformly weighted circular antennas for isotropic scattering ($\ell_x = \ell_y = \ell_0$). The antennas in this example are all pointed along the line of sight. The upper left plot is the same as in Figure 2.2 and is for a point antenna ($D \ll \ell_0$), for which there is no antenna filtering. The other three plots are for cases where the ratio of antenna diameter to decorrelation distance is equal to 1, 2, and 4. As the antenna size increases for a given value of ℓ_0 or, equivalently, as the decorrelation distance decreases for a given antenna diameter D , more of the energy arriving at large scattering angles is filtered out.

Antenna filtering has two major effects, one of which is generally bad and the other potentially good in terms of system performance. The bad effect is scattering loss. Energy that arrives at large angles is not captured by the relatively narrow beam

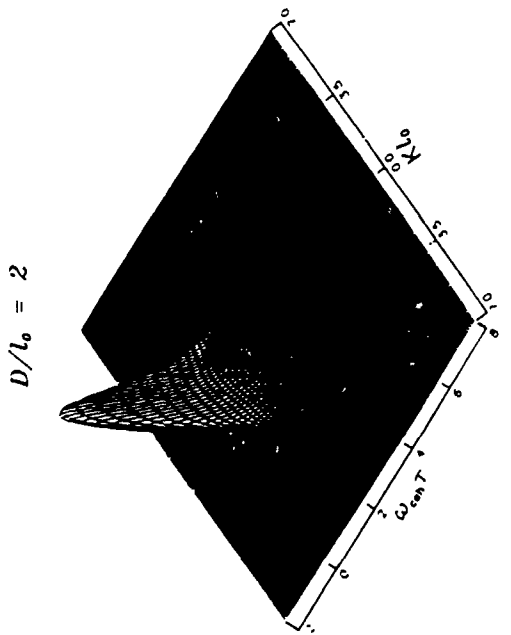
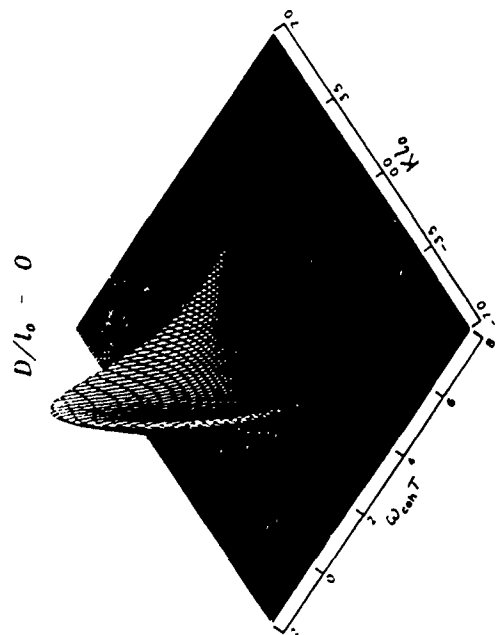
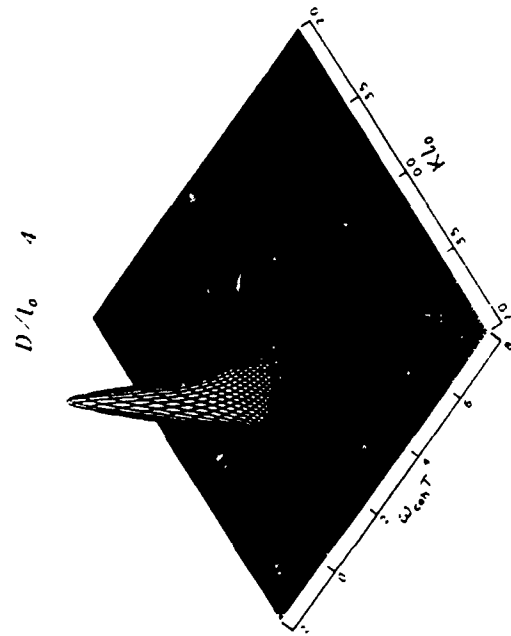
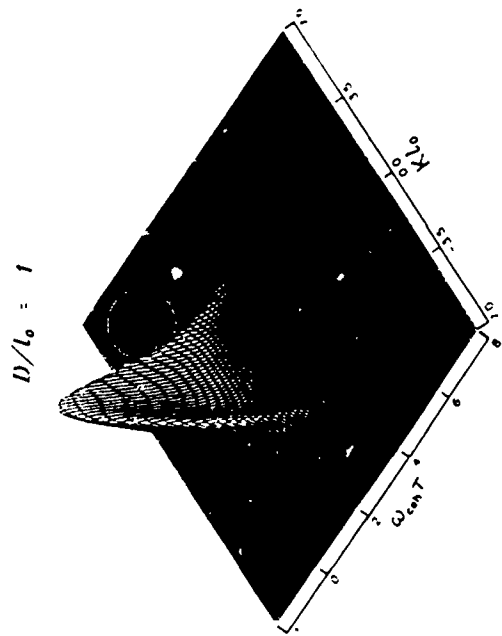


Figure 2.4. Generalized power spectra at the outputs of circular antennas.

of the large aperture antenna. An equivalent statement is that spatial decorrelation of the received electric field across the antenna aperture causes a reduction in the effective gain of the antenna. The magnitude of the scattering loss is a function of the ratio of the antenna diameter to decorrelation distance of the incident wave and a function of the pointing angle of the antenna beam away from the line of sight.

Figure 2.5 shows the scattering loss of a uniformly weighted circular antenna versus the ratio l_0/D when the pointing angle of the antenna beam is 0 , $\theta_0/2$ and θ_0 . It is assumed for this example that the beamwidth remains constant as the beam is pointed away from the line of sight. When the decorrelation distance is large compared to the antenna diameter, the curves approach the line of sight loss of beam (0 dB for 0 pointing angle, 3 dB for $\theta_0/2$ pointing angle, and 12 dB for θ_0 pointing angle). When the decorrelation distance is small compared to the antenna diameter, the angle of arrival spread of the incident energy is large compared to the beamwidth, so the scattering loss is insensitive to pointing angle as long as the pointing angle remains within a few beamwidths of the line of sight.

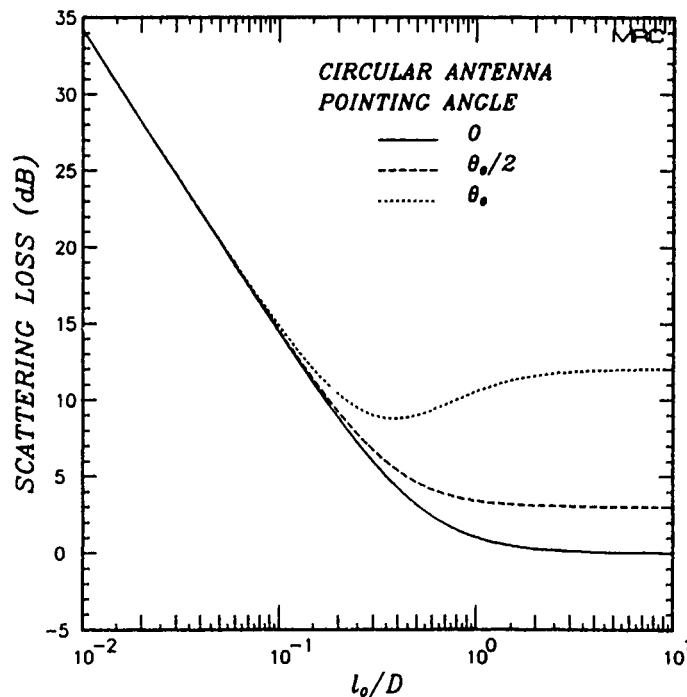


Figure 2.5. Scattering loss for a uniformly weighted circular antenna.

The potentially beneficial effect of antenna filtering is that the energy which is filtered out is that which arrives at relatively large delays. It is this delayed energy that causes most of the intersymbol interference in the detection and demodulation of wide bandwidth signals. Stated another way, because the antenna filters out much of the delayed energy, and since the frequency selective bandwidth is an inverse measure of the signal delay spread, the filtering increases the frequency selective bandwidth of the output signal relative that at the antenna input. This is shown in Figure 2.6, which has plots the ratio of the filtered to unfiltered frequency selective bandwidth, f_A/f_0 , as a function of the ratio l_0/D for a uniformly weighted circular antenna.

Figure 2.6 illustrates an interesting effect of pointing the beam away from the line of sight. As the pointing angle increases at a fixed value of the ratio l_0/D , the standard deviation of the time delay jitter increases and the filtered value of the frequency selective bandwidth decreases. Thus intersymbol interference effects in the output of a beam may increase as the beam is pointed away from the line of sight.

Antenna filtering can also affect the decorrelation time of the received signal as shown in Figure 2.7. The filtered value of decorrelation time is independent of pointing angle, but depends strongly on the model for the temporal fluctuations. For turbulent model, the Doppler spectrum is independent of angle, so the signal energy arriving at all angles has the same decorrelation time. Hence the filtered value of decorrelation time is equal to that of the incident signal ($\tau_A/\tau_0 = 1$) for this model. For the frozen-in model, there is strong coupling between the angular spectrum and the Doppler spectrum of the incident signal energy. The effect of an antenna is to narrow the angular spectrum the received signal energy as shown in Figure 2.4. Thus, for the frozen-in model, the antenna also narrows the Doppler spectrum of the received signal energy. Because the decorrelation time of the signal is an inverse measure of the width of the Doppler spectrum, the decorrelation time of the signal out of the antenna increases as antenna filtering effects increase. Reality should lie somewhere between these two limiting models.

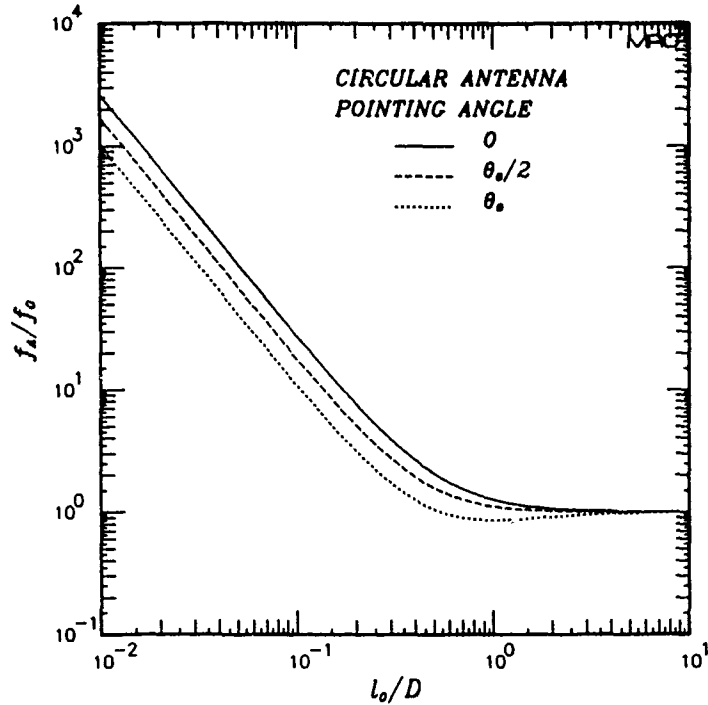


Figure 2.6. Filtered frequency selective bandwidth for a uniformly weighted circular antenna.

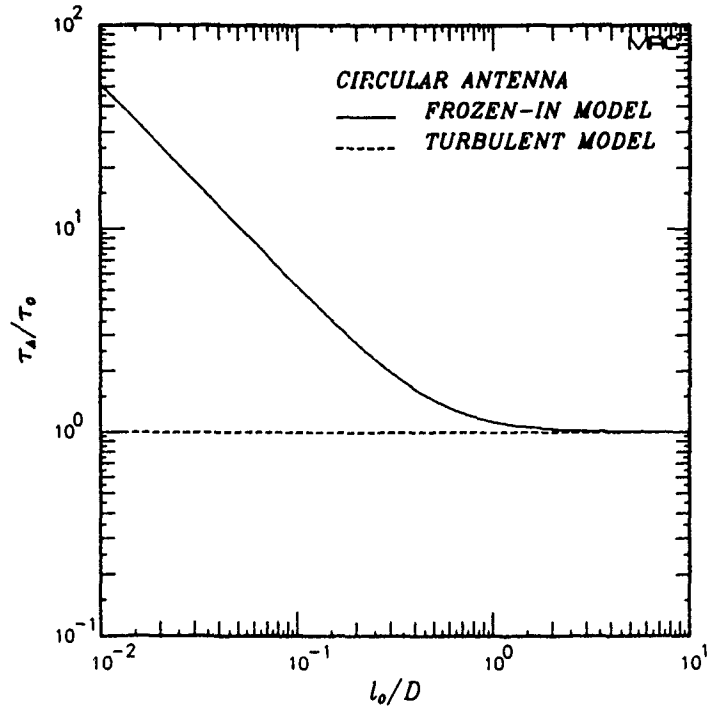


Figure 2.7. Filtered decorrelation time for a uniformly weighted circular antenna.

SECTION 3

CHANNEL SIMULATION

The purpose of this section is to describe statistical channel simulation techniques that allow realizations of the impulse response functions to be generated at the outputs of multiple antennas with spatial and temporal correlation properties given by the GPSD and with Rayleigh amplitude statistics. The realizations generated with these techniques represent only the diffractive part of the received voltage and are valid under strong scattering conditions where the GPSD is valid and where Rayleigh statistics apply. Under these conditions, the impulse response function represents a solution of Maxwell's equations for propagation of RF waves through randomly structured ionization.

The basic formalism to generate statistical realizations of the channel impulse response function without antenna effects explicitly included was developed by Wittwer (1980) for isotropic irregularities and was extended by Knepp (1982) to the case of elongated irregularities. (The elongated case corresponds to a 90° penetration angle and to an infinite axial ratio.) Channel simulation techniques have been generalized in ACIRF to include the effects of general anisotropic scattering and multiple receiving antennas.

Another extension of previous channel modeling techniques that is used in ACIRF is the use of the diffraction limited form of the GPSD (Equation 2.21). In this limit, there is a delta function relationship between scattering angle and delay. This allows the angular-delay part of the random signal to be generated in angle only. The relationship between angle and delay is then used to associate angular spectral components within an angular annulus to a unique delay bin. The advantage of this procedure is that it requires one less dimension in the arrays used for channel modeling thereby reducing both computation time and executable code size.

Channel simulation techniques rely on the assumptions that the channel is statistically stationary and that the first order statistics of the impulse response function are normal. The first step in channel modeling is to generate the random angular spectral components of the channel before the antennas. Because the channel is stationary in space, these components are uncorrelated from one angle to another. The angular spectrum of the channel is multiplied by the antenna beam profiles to produce the angular spectrum at the outputs of the antennas. The delta function relationship between angle and delay is used to associate the angular components with

unique delay bins. After this point, techniques used for the frozen-in and turbulent models to create signal temporal variations are quite different.

For the frozen-in model, temporal variations result from a drift of a random diffraction pattern across the receiving antennas. Of course it is equally valid to assume that the antennas drift past the random diffraction pattern. The latter viewpoint is used in the channel model. The impulse response functions are generated by fast Fourier transforming the angular spectra at the outputs of the antennas to a sequence of positions along the x axis. Temporal variations result by setting the relative speed between the diffraction pattern and the antennas to one decorrelation distance per decorrelation time (i.e. speed is equal to ℓ_x/τ_0). There is then a one-to-one relationship between the K_x angular spectrum, modified by K_x component the antenna beam profile, and the Doppler spectrum as described by Equation 2.9. The output of the channel model is the impulse response functions $h(j\Delta\tau, n\Delta t)$ for each antenna at a set of discrete times $n\Delta t$ and delays $j\Delta\tau$.

For the turbulent model, temporal variations in the impulse response function result from temporal variations in the random angular spectral components. An f^{-4} Doppler spectrum has been chosen for computational convenience. It is then possible to generate the temporal variations of the angular spectral components directly in the time domain by passing white Gaussian noise through two-pole low pass filters. At a given time, the angular spectral components of the channel are modified by the antenna beam profiles and divided into delay bins. Then discrete Fourier transforms are performed from the angular domain to the locations of the antennas. At the next time step, the angular spectral components of the channel are updated using the f^{-4} filters, modified by the antenna beam profiles, divided into delay bins, and Fourier transformed to the antenna positions, and so on. Again the output is the impulse response functions for each antenna at a set of discrete times and delays.

3.1 FROZEN-IN MODEL.

The steps used to generate realizations of the impulse response functions at the outputs of multiple antennas using the frozen-in model are outlined below. Further details of the algorithm may be found in Wittwer and Dana (1989).

3.1.1 Discrete Evaluation of the GPSD.

The first step in generating the impulse response function is the evaluation of the GPSD on a discrete angular-delay ($K_x - K_y - \tau$) grid. The angular-delay grid centers are defined by

$$\begin{aligned} K_x &= k\Delta K_x \\ K_y &= l\Delta K_y \\ \tau &= (j + 1/2)\Delta\tau \end{aligned} \quad (3.1)$$

where k , l , and j are integers. The angular and delay grid sizes and the requirements on the number of grid points will be discussed later. For the j^{th} delay bin, the GPSD will be non-zero only for the angles that satisfy the condition

$$j\omega_{coh}\Delta\tau \leq \frac{\Lambda (K_x^2 + K_y^2) \ell_x^2}{4} < (j + 1)\omega_{coh}\Delta\tau \quad (3.2)$$

where, for this diffraction limited case, ω_{coh} is equal to $2\pi f_0$.

The mean signal energy in a $K_x - K_y$ grid cell at the output of the m^{th} antenna is

$$E_m(k, l) = \int_{k-1/2}^{k+1/2} \frac{dK_x}{\Delta K_x} \int_{l-1/2}^{l+1/2} \frac{dK_y}{\Delta K_y} G_m(K_x - K_{0x}, K_y - K_{0y}) S_K(K_x, K_y) \quad (3.3)$$

where the angular power spectral density S_K is

$$S_K(K_x, K_y) = \int_{-\infty}^{\infty} S_{K\tau}(K_x, K_y, \tau) d\tau = \pi \ell_x \ell_y \exp \left[-\frac{K_x^2 \ell_x^2 + K_y^2 \ell_y^2}{4} \right] \quad (3.4)$$

Equation 3.3 is completely general, but it implies that $E_m(k, l)$ must be computed and stored for each separate antenna. If, however, it is assumed that the antenna beam profile is constant across a $K_x - K_y$ bin, then Equation 3.3 can be approximated by

$$E_m(k, l) = G_m(k\Delta K_x - K_{0x}, l\Delta K_y - K_{0y})E(k, l) \quad (3.5)$$

where

$$\begin{aligned} E(k, l) &= \int_{(k-1/2)\Delta K_x}^{(k+1/2)\Delta K_x} \frac{dK_x}{2\pi} \int_{(l-1/2)\Delta K_y}^{(l+1/2)\Delta K_y} \frac{dK_y}{2\pi} S_K(K_x, K_y) \\ &= \frac{1}{2} \left\{ \operatorname{erf} \left[\frac{(k+1/2)\Delta K_x \ell_x}{2} \right] - \operatorname{erf} \left[\frac{(k-1/2)\Delta K_x \ell_x}{2} \right] \right\} \times \\ &\quad \frac{1}{2} \left\{ \operatorname{erf} \left[\frac{(l+1/2)\Delta K_y \ell_y}{2} \right] - \operatorname{erf} \left[\frac{(l-1/2)\Delta K_y \ell_y}{2} \right] \right\} \end{aligned} \quad (3.6)$$

and where $\operatorname{erf}(\cdot)$ is the error function. The accuracy of this approximation and that of a few similar approximations to Equation 3.3 is discussed in Appendix B. It is shown in Appendix B that Equation 3.5 is generally accurate to within a small fraction of a percent.

3.1.2 Random Realizations of the Impulse Response Function.

The impulse response functions will be generated one delay at a time starting with the smallest delay ($j = 0$) and working to the largest delay ($j = j_{max}$). For each delay, the steps that are performed are outlined in this subsection.

The angular spectrum of the impulse response function in the j^{th} delay bin at the output of the m^{th} antenna is

$$\tilde{h}_m(k\Delta K_x, l\Delta K_y, j\Delta\tau) = \begin{cases} \frac{4\pi^2}{\Delta K_x \Delta K_y \Delta\tau} \xi(k, l) \sqrt{E_m(k, l)} & \text{if Eqn. 3.2} \\ 0 & \text{otherwise} \end{cases} \quad (3.7)$$

The normalization $4\pi^2/\Delta K_x \Delta K_y \Delta\tau$ is chosen so that when the Fourier transforms from angle to space are complete, the quantity $\tilde{h}_m(j\Delta\tau, k\Delta t)\Delta\tau$ will represent the received signal (without modulation included) during the delay interval $j\Delta\tau$ to $(j+1)\Delta\tau$.

The quantity $\xi(k, l)$ is a complex, zero mean, Gaussian random variable with the properties

$$\begin{aligned}\langle \xi(k, l) \xi^*(\alpha, \beta) \rangle &= \delta_{k, \alpha} \delta_{l, \beta} \\ \langle \xi(k, l) \rangle &= 0 \\ \langle \xi(k, l) \xi(\alpha, \beta) \rangle &= 0\end{aligned}\quad (3.8)$$

where $\delta_{k, l}$ is the Kronecker delta symbol. The random numbers ξ may be generated using the equation

$$\xi = \sqrt{-\ln u_1} \exp(2\pi i u_2) \quad (3.9)$$

where u_1 and u_2 are independent random numbers uniformly distributed on the interval $[0, 1)$.

There is no explicit y coordinate since realizations will be generated only at y coordinates corresponding to antenna centers. This is accomplished by first generating N_y samples of \tilde{h}_m in the K_y domain and then by Fourier transforming \tilde{h}_m to the y domain using discrete Fourier transforms (DFTs). One DFT is performed at each K_x coordinate grid point for each unique antenna center y coordinate. In continuous notation, this transform is

$$\tilde{h}_m(K_x, \tau) = \int_{-\infty}^{\infty} \exp(iK_y y_m) \tilde{h}_m(K_x, K_y, \tau) \frac{dK_y}{2\pi} \quad (3.10)$$

where y_m is the y coordinate of the m^{th} antenna center. The DFT equivalent of Equation 3.10 is

$$\tilde{h}_m(k\Delta K_x, j\Delta\tau) = \frac{\Delta K_y}{2\pi} \sum_{l=-N_y/2}^{N_y/2} \exp(il\Delta K_y y_m) \tilde{h}_m(k\Delta K_x, l\Delta K_y, j\Delta\tau) \quad (3.11)$$

Now the K_x to x Fourier transform is performed for each antenna. In this case, a fast Fourier transform (FFT) may be used. In continuous notation

$$h_m(x, \tau) = \int_{-\infty}^{\infty} \exp(iK_x x) \tilde{h}_m(K_x, \tau) \frac{dK_x}{2\pi} . \quad (3.12)$$

The discrete equivalent of Equation 3.12 is

$$h_m(k\Delta x, j\Delta\tau) = \frac{\Delta K_x}{2\pi} \sum_{k'=-N_x/2}^{N_x/2-1} \exp(ik'\Delta K_x k\Delta x) \tilde{h}_m(k'\Delta K_x, j\Delta\tau) \quad (3.13)$$

where N_x is the number of x coordinate grid points.

The quantity $h_m(k\Delta x, j\Delta\tau)$ is the impulse response function at the output of the m^{th} antenna when that antenna is located at x position $k\Delta x$. Under the frozen-in model, a time step Δt may be associated with Δx using the effective velocity:

$$\Delta t = \Delta x(\tau_0/\ell_x) . \quad (3.14)$$

Thus $h_m(k\Delta x, j\Delta\tau)$ also represents the impulse response function at the output of the m^{th} antenna at time $k\Delta t$.

3.1.3 Grid Sizes.

The angular grid sizes ΔK_x and ΔK_y are chosen so the magnitude of the antenna filtered GPSD will be negligible at the edges of the angular grid, and so there will be a sufficient number of samples per decorrelation distance to resolve the fades of the Rayleigh amplitude distribution.

The delay grid size $\Delta\tau$ is generally chosen on the basis of the sampling period of the receiver. The number of delay samples N_D of the realizations is then chosen so the total delay spread of the realization $N_D\Delta\tau$ will encompass at least 95 percent of the delayed signal energy.

K_x Grid

The x grid spacing is

$$\Delta x = \ell_{Ax}/N_0 \quad (3.15)$$

where ℓ_{Ax} is the minimum (of the values for all antennas) filtered x direction decorrelation distance. The quantity N_0 is the number of samples per decorrelation distance or time where N_0 should have a value of 10 or larger in order for the realization to accurately represent the duration and separation of the fades of the Rayleigh amplitude distribution (Dana 1982, 1988).

The number of x grid points N_x is subject to two constraints: First, N_x should be a power of 2 so a fast Fourier transform can be used to transform from the K_x domain to the x domain. Second, N_x should be greater than or equal to $100 N_0$. Equivalently, there should be at least 100 x direction decorrelation distances and therefore 100 decorrelation times in the realization in order for the realization to represent a reasonable sample of the random process.

Here reasonable is defined in terms of the application. Typically, the realizations are used to exercise simulations of trans-ionospheric communications links. Each realization with N_x/N_0 approximately equal to 100 can be used to calculate link performance averaged over 100 decorrelation times. The resulting receiver performance measures will have some statistical variation due to the finite time duration of the simulation. This variation can be reduced by either using longer realizations or by using several realizations with the same signal parameters but with different random numbers and by averaging the results from the multiple realizations. This latter approach allows an estimate of the statistical variation in the performance to be made.

Returning to the grid spacing, the x direction distance spanned by the realization is $L_x = N_x \Delta x$ and ΔK_x is

$$\Delta K_x = \frac{2\pi}{L_x} = \frac{2\pi}{N_x \Delta x} \quad (3.16)$$

The functional dependence of the antenna filtered GPSD on K_x is given approximately by $\exp[-(K_x \ell_{Ax}/2)^2]$. In discrete notation, $K_x = k \Delta K_x$ where $|k|$ has a maximum value of $N_x/2$. Using the maximum value for K_x of $N_x \Delta K_x/2$, the value of the GPSD at the edge of the K_x grid is proportional to $\exp[-(\pi N_0/2)^2]$ which is essentially equal to zero when N_0 equals 10.

K_y Grid

The number of K_y grid points is determined by requiring that the magnitude of the antenna filtered GPSD is small at the edge of the K_y grid. The functional dependence of the antenna filtered GPSD on K_y is given approximately by $\exp[-(K_y \ell_{Ay}/2)^2]$. A convenient minimum value of the antenna filtered GPSD at the edge of the K_y grid is $\exp(-\pi^2)$. Using this value results in the following condition on N_y :

$$N_y \geq \frac{4\pi}{\Delta K_y \ell_{Ay}} \quad (3.17)$$

where ℓ_{Ay} is the minimum (of the values for all antennas) filtered y direction decorrelation distance. It is desirable to minimize the number of K_y samples in order to minimize computer memory and execution time requirements. A reasonable minimum value for N_y is 32.

The ΔK_y grid spacing is then

$$\Delta K_y = \frac{2\pi}{L_y} \quad (3.18)$$

where the length L_y is chosen to be

$$L_y = \text{maximum} [16\ell_{Ay}, 4\text{maximum}(|y_m|)] \quad (3.19)$$

The first condition, $L_y = 16\ell_{Ay}$, results from letting $N_y = 32$ in Equation 3.17. The second condition, $L_y = 4 \text{ maximum} (|y_m|)$, is chosen to minimize aliasing of the impulse response functions of the two antennas with the largest separation in the y direction. If the value of L_y is determined by this latter condition, then the value of N_y will need to be larger than 32 in order to satisfy the condition on N_y given by Equation 3.17.

Delay Grid

The delay grid size is usually chosen so there are an integer number of delay samples in a modulation period. The number of delay samples is chosen so the delay spread of the realization, $N_D \Delta \tau$, will encompass at least 95 percent of the delayed energy. Without an antenna, 95 percent of the signal energy, under isotropic scattering conditions, arrives with delays in the range $-0.25 < \omega_{coh} \tau < 3.45$ when the

delay parameter α is set at its minimum value of 4 (Wittwer 1980). To be conservative, this same criterion is applied under all conditions. This will result in a delay spread that encompasses more than 95 percent of the energy for anisotropic scattering cases with antennas. The minimum number of delay samples required is then

$$N_D \geq \frac{3.7}{2\pi f_{A,\min} \Delta\tau} \quad (3.20)$$

where $f_{A,\min}$ is the minimum (of the values for all antennas) filtered value of the frequency selective bandwidth.

3.2 TURBULENT MODEL.

The starting point for the turbulent model is the angular spectrum of the impulse response function. At discrete time $n\Delta t$ ($\Delta t = \tau_0/N_0$), the angular components of the impulse response function at the output of the m^{th} antenna for j^{th} delay bin are

$$\tilde{h}_m(k\Delta K_x, l\Delta K_y, j\Delta\tau, n\Delta t) = \begin{cases} \frac{4\pi^2}{\Delta K_x \Delta K_y \Delta\tau} \xi(k, l, n) \sqrt{E_m(k, l)} & \text{if Eqn. 3.2} \\ 0 & \text{otherwise} \end{cases} \quad (3.21)$$

The difference between this equation and Equation 3.7 is that the random numbers $\xi(k, l, n)$ are now functions of time as well as angle. The impulse response functions at the outputs of multiple antennas are then generated from $\tilde{h}_m(k\Delta K_x, l\Delta K_y, j\Delta\tau, n\Delta t)$ by performing the following two discrete Fourier transforms:

$$h_m(j\Delta\tau, n\Delta t) = \frac{\Delta K_x \Delta K_y}{4\pi^2} \sum_{k=-N_x/2}^{N_x/2-1} \exp(ik\Delta K_x x_m) \times \sum_{l=-N_y/2}^{N_y/2-1} \exp(il\Delta K_y y_m) \tilde{h}_m(k\Delta K_x, l\Delta K_y, j\Delta\tau, n\Delta t) \quad (3.22)$$

where x_m and y_m are the $x - y$ coordinates of the m^{th} antenna position. The angular grid size ΔK_x for this model is chosen using the same criteria that were used above to select K_y .

At the next time step, $(n + 1)\Delta t$, the random numbers $\xi(k, l, n)$ are recalculated according to the Doppler frequency spectrum. The f^{-4} form for the Doppler spectrum is convenient because the random numbers $\xi(k, l, n)$ can be readily synthesized using two-pole low-pass filters (see, for example, Wittwer 1980).

Once the noise samples ξ have been updated, the impulse response functions at time $(n + 1)\Delta t$ are again calculated using Equation 3.22.

SECTION 4

EXAMPLES

Several examples of the received voltage out of a matched filter are presented in this section. These examples are intended to illustrate the effects of frequency and spatial selectivity and the differences between frozen-in and turbulent models. Examples for specific system applications may be found in Bogusch, et. al. (1981) and in Bogusch, Guigliano, and Knepp (1983).

4.1 MATCHED FILTER OUTPUT.

The output of a matched filter can be constructed by convolving the impulse response function of the channel and antenna with the combined impulse response function of the transmitter and receiver. A second approach is to construct the combined frequency response of the transmitter, channel, antenna, and receiver and then to Fourier transform that result to obtain the matched filter output. This latter approach is used for the examples presented in this section.

The starting point is to calculate the channel/antenna transfer function which is the Fourier transform of the impulse response function:

$$H(\omega, t) = \int_0^{\infty} h(\tau, t) \exp(-i\omega\tau) d\tau \quad (4.1)$$

This function represents the response of the channel and antenna at time t to a transmitted sinewave with radian frequency ω .

For a transmitted square pulse with a chip duration T_C , the voltage out of the matched filter at time t can be written as

$$u(\tau, t) = \int_{-\infty}^{\infty} M(\omega) H(\omega t) \exp(i\omega\tau) \frac{d\omega}{2\pi} \quad (4.2)$$

where τ is the time delay of the matched filter relative to the nominal time of arrival (e.g. the time of arrival under benign propagation conditions).

The combined spectrum of the transmitted square pulse and the receiver matched filter is

$$M(\omega) = T_C \frac{\sin^2(\omega T_C/2)}{(\omega T_C/2)^2} \quad (4.3)$$

The impulse response function is generated with N_D delay samples of size $\Delta\tau$, so the discrete channel/antenna transfer function has an unambiguous frequency response over $2\pi/\Delta\tau$ radians. If this bandwidth is divided into N_F frequency samples, then the channel/antenna transfer function at discrete time $n\Delta t$ is

$$H(k\Delta\omega, n\Delta t) = \sum_{j=0}^{N_D-1} [h(j\Delta\tau, n\Delta t)\Delta\tau] \exp[-i(k - N_F/2)\Delta\omega j\Delta\tau] \quad (4.4)$$

where $\Delta\omega = 2\pi/(N_F\Delta\tau)$. The range of the index k in this equation is from 0 to $N_F - 1$ representing a range of frequencies from $-N_F\Delta\omega/2$ to $(N_F - 1)\Delta\omega/2$. Of course the number of frequency samples should be at least as large as the number of delay samples. However, if the number of delay samples was chosen to be the minimum number required by Equation 3.21, then it may be necessary to choose the number of frequency samples to be larger than the number of delay samples in order to minimize aliasing (in delay) of the matched filter output.

The output voltage of the matched filter as a function of time and relative delay is given by

$$u(\tau, n\Delta t) = \frac{\Delta\omega T_C}{2\pi} \sum_{k=-N_F/2}^{N_F/2-1} \left[\frac{\sin^2(k\Delta\omega T_C/2)}{(k\Delta\omega T_C/2)^2} \right] H(k\Delta\omega, n\Delta t) \exp(ik\Delta\omega\tau) \quad (4.5)$$

If $\Delta\tau$ is chosen to be $T_C/2$, then $\Delta\omega T_C/2 = 2\pi/N_F$ and $u(\tau, t)$ represents a signal that is band-limited to the frequency range $-1/T_C$ to $+1/T_C$. Note that the matched filter output $u(\tau, t)$ is unambiguous in delay over the interval from 0 to $(N_F - 1)\Delta\tau$ compared to the delay interval of 0 to (N_D-1) for the original ACIRF realization.

4.2 SCINTILLATION EFFECTS ON MATCHED FILTER OUTPUT.

In the examples that follow, the chip rate R_C is set at 1 Mhz, and the random realizations of the impulse response function are generated with a delay sample size of $T_C/2$ ($T_C = 1/R_C$). However, the frequency selective effects depend only on the ratio of the frequency selective bandwidth to the chip rate f_0/R_C . For the antenna examples, a uniformly weighted circular antenna and isotropic scattering are assumed. Antenna effects then depend only on the ratio of the antenna diameter D to the decorrelation distance ℓ_0 and the antenna pointing angle.

4.2.1 Frequency Selective Effects.

In a high data rate communications link, the major effect of frequency selective fading is intersymbol interference. Even relatively small amounts of delay spread can catastrophically degrade demodulation performance in such a link using conventional matched filter detection techniques.

Figure 4.1 shows examples of the matched filter output amplitude for three levels of frequency selective propagation disturbances, characterized by the ratio of the frequency selective bandwidth f_0 to the chip rate R_C .

The impulse response functions were generated using the frozen-in model and a small antenna (i.e. $D \ll \ell_0$). Each frame in the figure provides a three dimensional picture of the matched filter output for a single transmitted pulse as a function of time delay (abscissa) and time (scale directed into the figure). The total duration of each of the frames is 10 decorrelation times.

In the top frame the frequency selective bandwidth is equal to the chip rate and only a small amount of distortion is evident in the waveform (which is slightly rounded due to band limiting at the first nulls of the signal spectrum). The effect of fading can be seen in this frame as the peak amplitude rises and falls with time. Some minor distortion of the output amplitude is seen but for the most part the signal is contained within the period of one chip. This channel is nearly flat fading which means that all frequency components within the signal bandwidth propagate essentially the same way through the disturbed ionosphere. There is very little time delay spread beyond one chip in the matched filter output.

The middle frame in Figure 4.1 shows the matched filter output amplitude for the case where f_0/R_C is equal to 0.2. For this smaller value of the frequency selective

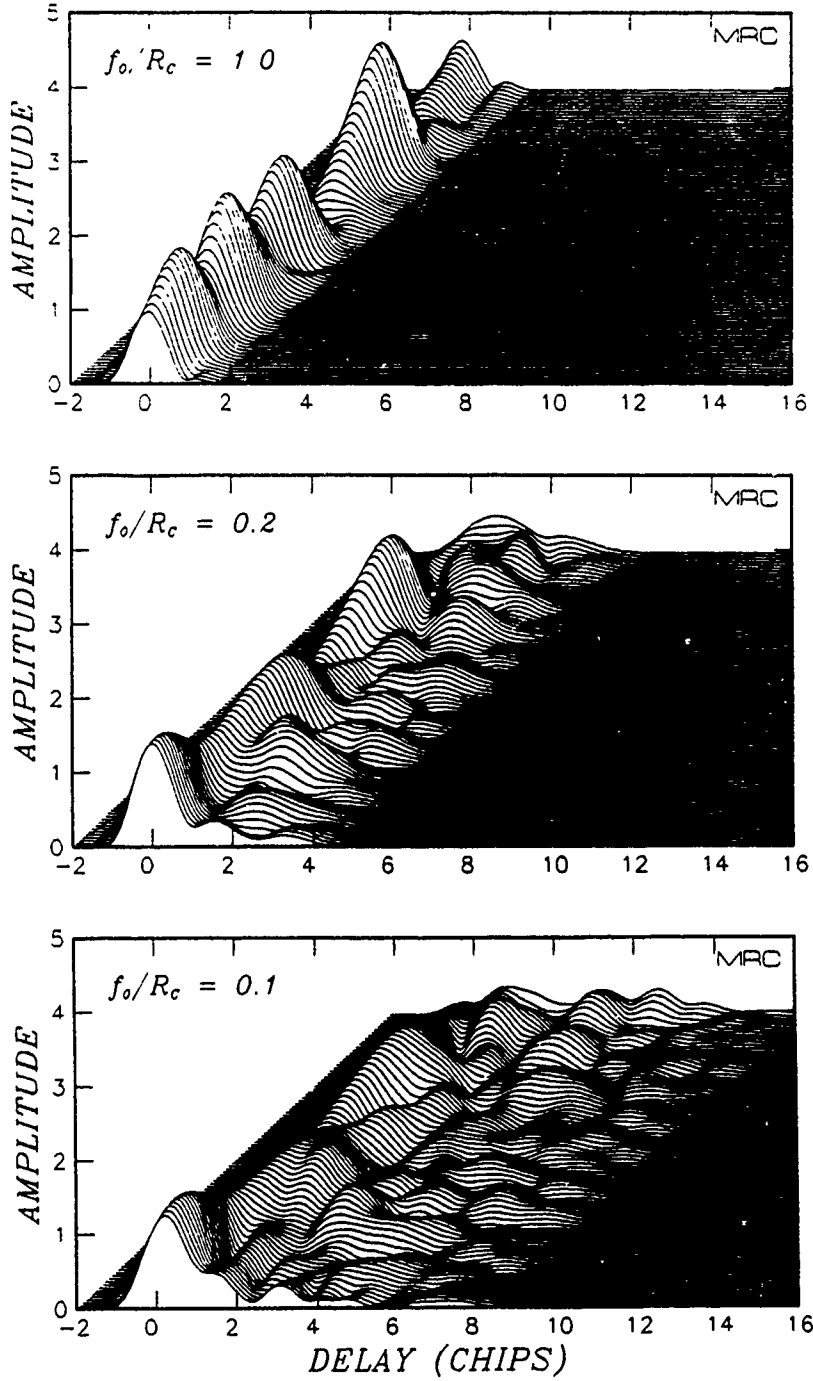


Figure 4.1. Effects of frequency selective fading.

bandwidth, more of the signal energy is arriving with delays of more than one chip, and there are multiple distinct peaks in the matched filter output amplitude. It is these structures that can cause delay tracking algorithms to lose lock and that cause intersymbol interference which can degrade demodulation performance.

The bottom frame shows a highly disturbed case where f_0 is a tenth of the chip rate. This causes signal energy to be spread over approximately eight chip periods. When a contiguous set of pulses is transmitted, the delay spread of the received signal results in the simultaneous reception of information from about eight previous chips which can produce severe intersymbol interference.

An effect due to the frozen-in model that is evident in Figure 4.1 is that the signal arriving at long delays varies more rapidly in time than the signal arriving at shorter delays. A comparison of the matched filter output amplitude generated with the frozen-in and turbulent models is shown in Figure 4.2 for the case where f_0/R_C is equal to 0.1. The top frame in this figure for the frozen-in model is just a reproduction of the bottom frame in Figure 4.1. Again 10 decorrelation times of the signal are plotted. It should be recalled when comparing the two frames that the Doppler spectrum for the frozen-in model has a Gaussian form, and the Doppler spectrum for the turbulent model has the f^{-4} form. It is this fact that accounts for the more spiky appearance of the turbulent model output amplitude. The important difference between the two frames is that the turbulent model amplitude has the same fading rate at all delays.

4.2.2 Spatially Selective Effects.

Spatially selective effects are important for high data rate communications links that rely on large antennas to achieve sufficient signal-to-noise ratios for low error rate data demodulation. Scattering loss of an antenna is a function of the size of the antenna D relative to the decorrelation distance, ℓ_0 . When ℓ_0 is greater than D , the electric field is highly correlated across the face of the antenna and the full gain of the antenna is realized. However, the antenna may be located at a position where the incident power is in a deep fade. The solution to this problem is to have multiple antennas physically separated by a distance larger than the maximum decorrelation distance. The probability of having all antennas simultaneously experience deep fades in the received power is then substantially reduced.

The problem of spatial selectivity occurs when ℓ_0 is less than D and the electric field is decorrelated across the face of the antenna. In this case, the induced

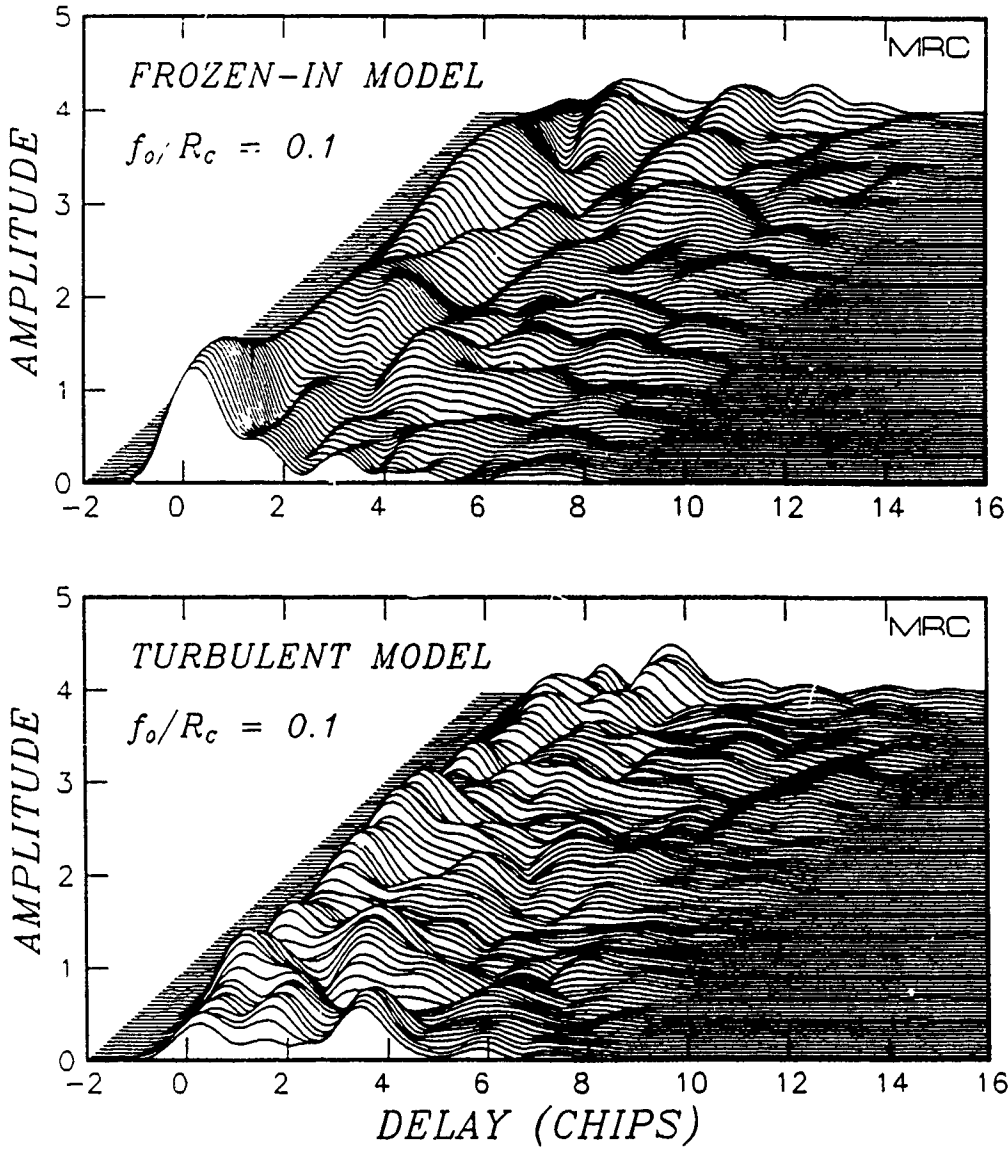


Figure 4.2. Comparison of matched filter output amplitude for the frozen-in and turbulent models.

voltages in the antenna add noncoherently due to the random phase variations in the electric field, and a loss of signal power, or equivalently of antenna gain, is the result. From another perspective, this loss occurs when the angular scattering process responsible for amplitude and phase scintillation and frequency selective effects also causes some of the transmitted signal energy to be scattered out of the antenna beam.

Figure 4.3 shows examples of the matched filter output amplitude for three levels of spatially selective propagation disturbance, characterized by the ratio of the antenna size to the decorrelation distance. The ratio of the frequency selective bandwidth to the chip rate is 0.1, and the antenna is pointing along the line of sight. The top frame is for the case where ℓ_0 is much greater than D , and is just a reproduction of the bottom frame of Figure 4.1. The middle frame is for a ℓ_0/D ratio of 0.5 where the scattering loss is 3.1 dB. The effect of the antenna is to preferentially attenuate the signal energy arriving at large angles and also at large delays and thereby to reduce the delay spread of the output signal. In the bottom frame where ℓ_0/D is equal to 0.2, the output signal is almost flat with very little delay spread distortion of the matched filter output. Although this substantially reduces the effects of frequency selective fading, the cost is an 8.8 dB reduction in the average signal power.

Finally, Figure 4.4 shows examples of the matched filter output amplitude for three values of the pointing angle ψ . The ratio of the frequency selective bandwidth to the chip rate is 0.1, and the ratio of decorrelation distance to antenna diameter is 0.5. The top frame for a pointing angle of zero is just a reproduction of the middle frame of Figure 4.3. The average scattering loss for this case is 3.1 dB. The bottom two frames show the matched filter output amplitude for pointing angles of one-half beamwidth ($\psi = \theta_0/2$) with a scattering loss of 4.6 dB and one beamwidth ($\psi = \theta_0$) with a scattering loss of 9.2 dB.

Although the average scattering losses are about the same, the bottom frame of Figure 4.4 ($\ell_0/D = 0.5$ and $\psi = \theta_0$) and the bottom frame of Figure 4.3 ($\ell_0/D = 0.2$ and $\psi = 0$) are qualitatively quite different. For the case with the pointing angle equal to a beamwidth, the received power is much more spread out in delay compared to the case with zero pointing angle where the signal energy is concentrated near zero delay. This is due to the fact that the antenna pointed away from the line of sight has relatively higher gain at large angles and long delays and relatively lower gain at small angles and short delays than does an antenna pointed along the line of sight. Thus for an antenna pointed away from the line of sight, increased scattering loss does not necessarily result in reduced frequency selective effects.

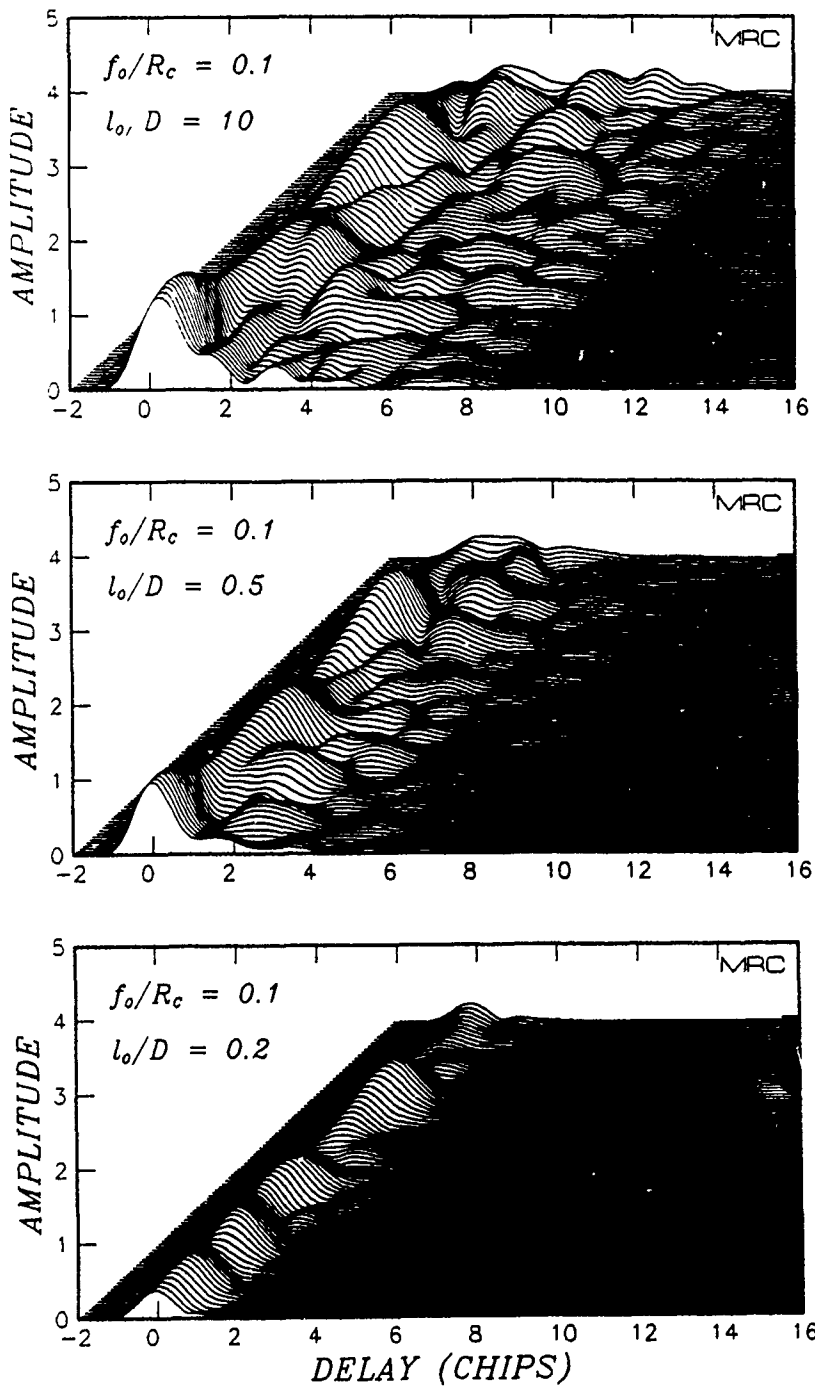


Figure 4.3. Effects of spatially selective fading.

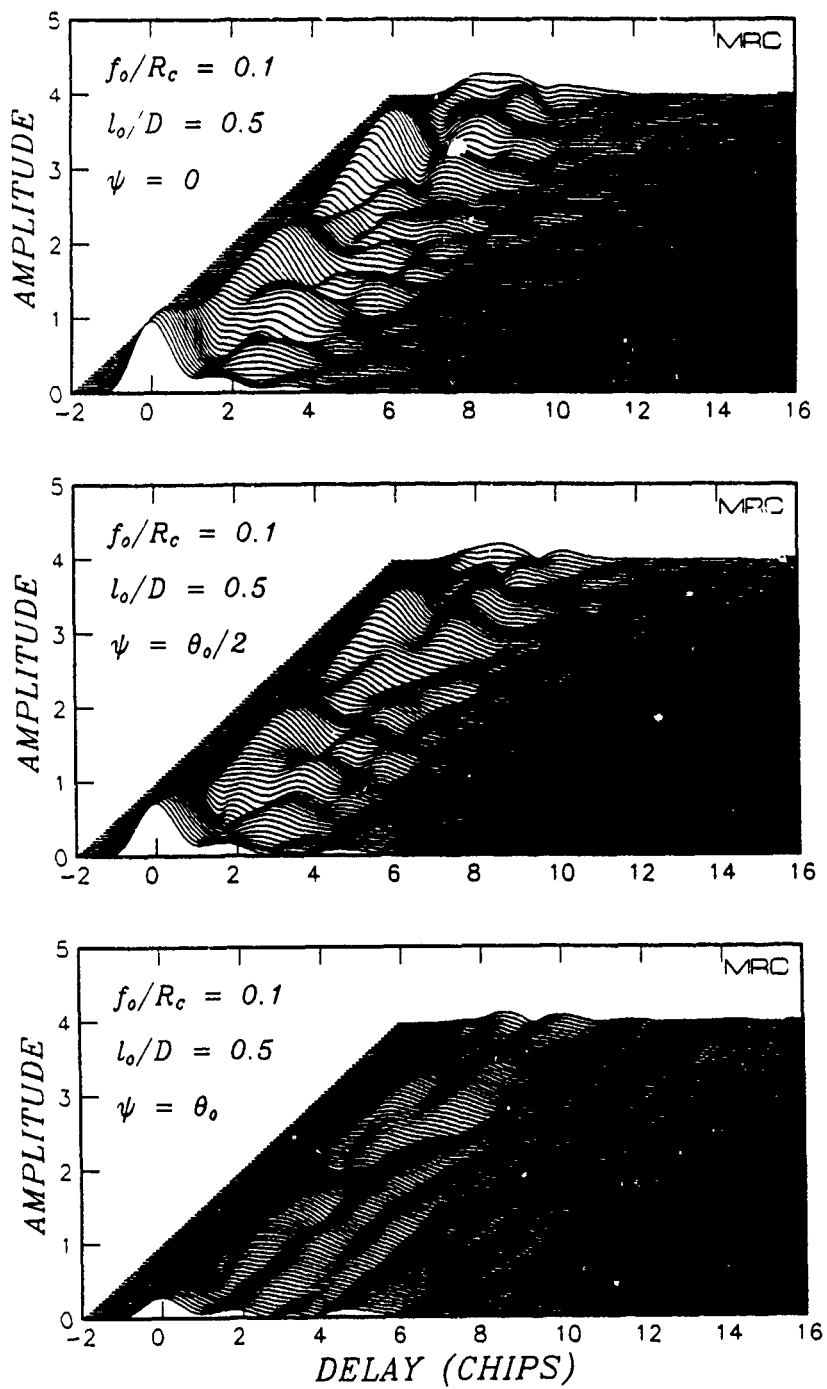


Figure 4.4. Effects of beam pointing.

SECTION 5
LIST OF REFERENCES

Bogusch, R. L., F. W. Guigliano, D. L. Knepp, and A. H. Michelet, "Frequency Selective Propagation Effects on Spread-Spectrum Receiver Tracking," *Proc. IEEE*, Vol. 69, No. 7, pp. 787-796, July 1981.

Bogusch, R. L., F. W. Guigliano, and D. L. Knepp, "Frequency Selective Scintillation Effects and Decision Feedback Equalization in High Data-Rate Satellite Links," *Proc. IEEE*, Vol. 71, No. 6, pp. 754-767, June 1983.

Dana, R. A., *Temporal Statistics of Scintillation for Satellite Communications and Radar Systems*, DNA-TR-81-129, MRC-R-692, Mission Research Corporation, April 1982.

Dana, R. A., *Propagation of RF Signals Through Structured Ionization. Theory and Antenna Aperture Effect Applications*, DNA-TR-86-158, MRC-R-976, Mission Research Corporation, May 1986.

Dana, R. A., *Statistics of Sampled Rayleigh Fading*, MRC-R-1023, Mission Research Corporation, April 1988.

Frasier, S. M., *The Effects on Antenna Filtered Scintillation Parameters of Non-Zero Antenna Pointing Angles*, MRC-R-1220, Mission Research Corporation, February 1989.

Knepp, D. L., *Propagation of Wide Bandwidth Signals Through Strongly Turbulent Ionized Media*, DNA-TR-81-87, MRC-R-671, Mission Research Corporation, March 1982.

Knepp, D. L., and L. A. Wittwer, "Simulation of Wide Bandwidth Signals That Have Propagated Through Random Media," *Radio Science*, Vol. 19, No. 1, pp. 302-318, January 1984.

Wittwer, L. A., *A Trans-Ionospheric Signal Specification for Satellite C^s Applications*, DNA 5662D, Defense Nuclear Agency, December 1980.

Wittwer, L. A., *Private Communication*, January 1988.

Wittwer, L. A., *Private Communication*, January 1989.

Wittwer, L. A., and R. A. Dana, *A Trans-Ionospheric Signal Specification for Satellite C^s and Radar Applications*, Defense Nuclear Agency, (in Preparation), 1989.

APPENDIX A

INPUTS AND OUTPUTS OF ACIRF

A.1 ACIRF INPUT FILE.

The key inputs to ACIRF are listed in Table A.1. These include channel parameters which describe the second order statistics of the signal incident on the face of any antenna, antenna parameters, and realization parameters.

There are five channel models included in ACIRF: frozen-in model with antennas (IFADE = 1); turbulent model with antennas (IFADE = 2); frozen-in model without antennas (IFADE = 3); turbulent model without antennas (IFADE = 4); and a flat fading model (IFADE = 5). Models 3 and 5 are also implemented in Wittwer's channel model CIRF (Wittwer 1980).

The key realization parameter inputs are the number of delay samples and the delay sample size. The delay sample size should be no larger than one-half of the chip period. For most applications, setting Δr equal to $T_C/2$ is sufficient. The number of delay samples required is determined from Equation 3.21.

An example input file is listed in Table A.2. This input file was used to generate realizations of the impulse response function from which the plots in Figure 4.4 were created. Note that comment lines in the input file start with a semicolon (;).

A.2 FORMATTED ACIRF OUTPUT FILE.

The formatted output file generated using the example ACIRF data file is listed in Table A.3a. The first page of this file provides a summary of the inputs and lists, for each antenna, ensemble values of scattering loss, and filtered frequency selective bandwidth, decorrelation distances, and decorrelation time. Subsequent pages of the output file list, for each antenna, the measured values of these quantities. The last page lists ensemble and measured values for the cross correlation of the signal out of the antennas. The algorithms used to measure these quantities are given in Dana (1986).

Table A.1. Key ACIRF inputs.

<u>Channel Parameters:</u>	
Channel model, IFADE	
Frequency Selective Bandwidth, f_0	(Hertz)
Decorrelation Distances, ℓ_x and ℓ_y	(meters)
Decorrelation Time, τ_0	(seconds)
<u>Antenna Parameters:</u>	
Beamwidths, θ_{ou} and θ_{ov}	(degrees)
Positions, u and v	(meters)
Rotation angle, χ	(degrees)
Pointing angle, ψ	(degrees)
Pointing azimuth, ϵ	(degrees)
<u>Realization Parameters:</u>	
Number of delay samples, N_D	
Delay sample size, $\Delta\tau$	(seconds)

For each delay bin, amplitude moments and the scintillation index S_4 of the impulse response function are measured and output in the formatted file. The ensemble power in the j^{th} delay bin for the m^{th} antenna is

$$P_{mj} = \int_{j\Delta\tau}^{(j+1)\Delta\tau} P_m(\tau) d\tau \quad (\text{A.1})$$

for $j = 0, 1, \dots, N_D-1$. The power impulse response function $P_m(\tau)$ is

$$P_m(\tau) = \int_{-\infty}^{\infty} \frac{dK_x}{2\pi} \int_{-\infty}^{\infty} \frac{dK_y}{2\pi} G_m(K_x - K_{0x}, K_y - K_{0y}) S_{kr}(K_x, K_y, \tau) \quad , \quad (\text{A.2})$$

and is given in Frasier (1989). The ensemble values of the amplitude moments are

Table A.2. Example ACIRF input file.

```

: THIS DATA FILE IS FOR ACIRF USER'S GUIDE EXAMPLES
:
: ***** CASE NUMBER
:
: KASE
: 1001/
:
: ***** ALPHANUMERIC IDENTIFICATION (80 CHARACTERS OR LESS ENCLOSED IN ' ')
:
: 'ACIRF USERS GUIDE EXAMPLES'
:
: ***** CHANNEL PARAMETERS
:
: IFADE FO(HZ) TAUO(S) DLX(M) DLY(M)
: 1 0.1E6 3.0E-3 5.0 5.0/
:
: ***** ANTENNA PARAMETERS (READ ONLY IF IFADE = 1 OR IFADE = 2)
:
: NUMANT FREQC(HZ)
: 3 2.99793E9/
:
: BEAMWIDTHS, POSITIONS, ROTATION ANGLES, AND POINTING ANGLES
: (ONE LINE FOR EACH ANTENNA)
:
: BWU(DEG) BWV(DEG) UPOS(M) VPOS(M) CHI(DEG) PSI(DEG) EPS(DEG)
: 0.5896 0.5896 0.0 0.0 00.0 0.0 0.0/
: 0.5896 0.5896 0.0 0.0 00.0 0.2948 0.0/
: 0.5896 0.5896 0.0 0.0 00.0 0.5896 0.0/
:
: ***** REALIZATION PARAMETERS
:
: NDELAY DELTAU(S) NTIMES NKX NKY ISEED NO
: 16 5.0E-7 1024 1024 33 9771975 10/

```

Table A.3a. Example ACIRF output file (page 1, summary of input and ensemble values).

ACIRF CHANNEL SIMULATION

CASE NUMBER 1001
 TEMPORAL VARIATION FROM FROZEN-IN MODEL
 REALIZATION IDENTIFICATION:
 ACIRF USERS GUIDE EXAMPLES

CHANNEL PARAMETERS

FREQUENCY SELECTIVE BANDWIDTH (HZ) = 1.000E+05
 DECORRELATION TIME (SEC) = 3.000E-03
 X DECORRELATION DISTANCE (M) = 5.000E+00
 Y DECORRELATION DISTANCE (M) = 5.000E+00

REALIZATION PARAMETERS

NUMBER OF DELAY SAMPLES = 16
 DELAY SAMPLE SIZE (SEC) = 5.000E-07
 NUMBER OF TEMPORAL SAMPLES = 1024
 NUMBER OF KX SAMPLES = 1024
 NUMBER OF KY SAMPLES = 33
 INITIAL RANDOM NUMBER SEED = 9771975
 NUMBER OF TEMPORAL SAMPLES PER TAUO = 10

ANTENNA PARAMETERS

NUMBER OF ANTENNAS = 3
 CARRIER FREQUENCY (HZ) = 2.998E+09

ANTENNA BEAMWIDTHS, ROTATION ANGLES AND POINTING ANGLES

N	BWU(DEG)	BWV(DEG)	CHI(DEG)	PSI(DEG)	EPS(DEG)
1	.590	.590	.000	.000	.000
2	.590	.590	.000	.295	.000
3	.590	.590	.000	.590	.000

ANTENNA POSITIONS IN U-V AND X-Y COORDINATES

N	UPOS(M)	VPOS(M)	XPOS(M)	YPOS(M)
1	.000E+00	.000E+00	.000E+00	.000E+00
2	.000E+00	.000E+00	.000E+00	.000E+00
3	.000E+00	.000E+00	.000E+00	.000E+00

ENSEMBLE CHANNEL PARAMETERS AT ANTENNA OUTPUTS

N	LOSS(DB)	POWER	FA(HZ)	ALX(M)	ALY(M)	TAUA(SEC)
1	3.141	.485167	2.061E+05	7.178E+00	7.178E+00	4.307E-03
2	4.602	.346611	1.574E+05	7.178E+00	7.178E+00	4.307E-03
3	8.983	.126390	1.050E+05	7.178E+00	7.178E+00	4.307E-03

Table A.3b. Example ACIRF output file (page 2, summary for antenna 1).

```

MEASURED PARAMETERS FOR REALIZATION/ANTENNA 1

MOMENTS OF VOLTAGE AMPLITUDE VERSUS DELAY
NORMALIZED TO ENSEMBLE VALUES
POW(J) = ENSEMBLE POWER IN J-TH DELAY BIN
J = T: STATISTICS OF COMPOSITE SIGNAL

  J    POW(J)    <A> <A**2> <A**3> <A**4>    S4
  0  2.313E-01  .9568  .9500  .9780  1.0344  1.1368
  1  1.210E-01  1.0182  .9797  .8954  .7833  .7951
  2  6.334E-02  1.0642  1.1008  1.1242  1.1372  .9365
  3  3.315E-02  .9853  .9865  .9918  .9932  1.0203
  4  1.735E-02  .9251  .8651  .8137  .7675  1.0252
  5  9.078E-03  .9740  .9333  .8820  .8206  .9404
  6  4.751E-03  .9902  .9510  .8917  .8188  .9005
  7  2.486E-03  .9874  1.0009  1.0246  1.0525  1.0494
  8  1.301E-03  .9603  .9393  .9275  .9159  1.0373
  9  6.810E-04  .8717  .7371  .6098  .4952  .9071
 10  3.564E-04  1.0041  1.0300  1.0711  1.1248  1.0585
 11  1.865E-04  1.0205  1.0373  1.0546  1.0750  .9991
 12  9.761E-05  .9761  .9463  .9068  .8570  .9560
 13  5.108E-05  1.1056  1.1900  1.2640  1.3378  .9431
 14  2.673E-05  .9194  .8846  .8996  .9607  1.2063
 15  1.399E-05  1.0141  1.0324  1.0470  1.0563  .9910
  T  4.352E-01  .9973  .9651  .9071  .8270  .8808

MEASURED REALIZATION SIGNAL PARAMETERS

MEAN POWER OF REALIZATION          = .473660
TOTAL SCATTERING LOSS (DB)         = 3.245
FREQUENCY SELECTIVE BANDWIDTH (HZ) = 2.132E+05
X DIRECTION DECORR. DISTANCE (M)   = 7.325E+00
NUMBER OF SAMPLES PER DECORR. DIST = 10.205
DECORRELATION TIME (SEC)           = 4.395E-03

MEAN POWER IN GRID

POWER IN KX-KY GRID                = .484762
POWER LOSS OF GRID (DB)            = .004
POWER IN DELAY GRID                = .485152

```

Table A.3c. Example ACIRF output file (page 3, summary for antenna 2).

MEASURED PARAMETERS FOR REALIZATION/ANTENNA 2

MOMENTS OF VOLTAGE AMPLITUDE VERSUS DELAY

NORMALIZED TO ENSEMBLE VALUES

POW(J) = ENSEMBLE POWER IN J-TH DELAY BIN

J = T: STATISTICS OF COMPOSITE SIGNAL

J	POW(J)	<A>	<A**2>	<A**3>	<A**4>	S4
0	1.280E-01	.9974	1.0276	1.0774	1.1387	1.0756
1	8.257E-02	1.0332	1.0292	.9922	.9301	.8696
2	5.231E-02	1.0047	1.0114	1.0137	1.0034	.9807
3	3.267E-02	.9067	.8624	.8534	.8699	1.1572
4	2.017E-02	.9005	.8167	.7400	.6690	1.0029
5	1.233E-02	.8829	.7841	.6953	.6170	1.0036
6	7.476E-03	.9827	.9563	.9247	.8834	.9653
7	4.501E-03	.9811	.9739	.9699	.9628	1.0150
8	2.693E-03	1.0053	1.0322	1.0719	1.1137	1.0442
9	1.603E-03	.7867	.6194	.4785	.3586	.9324
10	9.495E-04	1.0011	1.0165	1.0284	1.0235	.9905
11	5.600E-04	1.0708	1.0918	1.0803	1.0432	.8661
12	3.290E-04	1.0146	.9520	.8434	.7138	.7583
13	1.926E-04	1.2411	1.4731	1.6962	1.9090	.8715
14	1.124E-04	1.0238	.9946	.9298	.8416	.8377
15	6.538E-05	.9993	.9598	.8861	.7892	.8447
T	3.465E-01	.9600	.9090	.8500	.7840	.9474

MEASURED REALIZATION SIGNAL PARAMETERS

MEAN POWER OF REALIZATION = .341379
 TOTAL SCATTERING LOSS (DB) = 4.668
 FREQUENCY SELECTIVE BANDWIDTH (HZ) = 1.637E+05
 X DIRECTION DECORR. DISTANCE (M) = 8.476E+00
 NUMBER OF SAMPLES PER DECORR. DIST = 11.808
 DECORRELATION TIME (SEC) = 5.086E-03

MEAN POWER IN GRID

POWER IN KX-KY GRID = .346241
 POWER LOSS OF GRID (DB) = .005
 POWER IN DELAY GRID = .346521

Table A.3d. Example ACIRF output file (page 4, summary for antenna 3).

MEASURED PARAMETERS FOR REALIZATION/ANTENNA 3						
MOMENTS OF VOLTAGE AMPLITUDE VERSUS DELAY						
NORMALIZED TO ENSEMBLE VALUES						
POW(J) = ENSEMBLE POWER IN J-TH DELAY BIN						
J = T: STATISTICS OF COMPOSITE SIGNAL						
J	POW(J)	<A>	<A**2>	<A**3>	<A**4>	S4
0	2.135E-02	1.0277	1.0802	1.1302	1.1686	1.0015
1	2.181E-02	1.0568	1.0626	1.0300	.9706	.8482
2	1.958E-02	.9992	.9990	.9907	.9674	.9690
3	1.630E-02	.8718	.8152	.8023	.8213	1.2132
4	1.291E-02	.8619	.7608	.6767	.6009	1.0373
5	9.851E-03	.8753	.7757	.6851	.6052	1.0058
6	7.308E-03	.9679	.9450	.9260	.8964	1.0038
7	5.300E-03	.9991	1.0150	1.0123	.9838	.9539
8	3.772E-03	1.0026	1.0523	1.1282	1.2156	1.0934
9	2.643E-03	.7554	.5634	.4070	.2825	.8834
10	1.827E-03	1.0246	1.0423	1.0436	1.0173	.9342
11	1.248E-03	1.0900	1.1059	1.0637	.9779	.7739
12	8.439E-04	1.0133	.9423	.8212	.6775	.7254
13	5.653E-04	1.2884	1.5853	1.8641	2.1096	.8239
14	3.756E-04	1.0628	1.0494	.9860	.8920	.7875
15	2.477E-04	1.0050	.9720	.8980	.7922	.8228
T	1.259E-01	.9246	.8494	.7772	.7086	.9820

MEASURED REALIZATION SIGNAL PARAMETERS	
MEAN POWER OF REALIZATION	= .119903
TOTAL SCATTERING LOSS (DB)	= 9.212
FREQUENCY SELECTIVE BANDWIDTH (HZ)	= 1.061E+05
X DIRECTION DECORR. DISTANCE (M)	= 7.308E+00
NUMBER OF SAMPLES PER DECORR. DIST	= 10.181
DECORRELATION TIME (SEC)	= 4.385E-03

MEAN POWER IN GRID	
POWER IN KX-KY GRID	= .125826
POWER LOSS OF GRID (DB)	= .019
POWER IN DELAY GRID	= .125933

Table A.3e. Example ACIRF output file (page 7, ensemble and measured antenna output cross correlation coefficients).

ENSEMBLE ANTENNA OUTPUT CROSS CORRELATION			
AMPLITUDE OF CROSS CORRELATION			
N	AMP(N-1)	AMP(N-2)	AMP(N-3)
1	1.000000	.914651	.699883
2	.914651	1.000000	.914655
3	.699883	.914655	1.000000
PHASE (RADIANS) OF CROSS CORRELATION			
N	PHS(N-1)	PHS(N-2)	PHS(N-3)
1	.000000	.000000	.000000
2	.000000	.000000	.000000
3	.000000	.000000	.000000
MEASURED ANTENNA OUTPUT CROSS CORRELATION			
AMPLITUDE OF CROSS CORRELATION			
N	AMP(N-1)	AMP(N-2)	AMP(N-3)
1	1.000000	.916112	.703803
2	.916112	1.000000	.914799
3	.703803	.914799	1.000000
PHASE (RADIANS) OF CROSS CORRELATION			
N	PHS(N-1)	PHS(N-2)	PHS(N-3)
1	.000000	.000000	.000000
2	.000000	.000000	.000000
3	.000000	.000000	.000000
FINAL RANDOM NUMBER SEEDS			
ISEED =	26550		
JSEED =	63489		

$$\begin{aligned}
\langle a_j \rangle &= \frac{1}{2} \sqrt{\pi P_{mj}} \\
\langle a_j^2 \rangle &= P_{mj} \\
\langle a_j^3 \rangle &= \frac{3}{4} \sqrt{\pi P_{mj}^3} \\
\langle a_j^4 \rangle &= 2P_{mj}^2 .
\end{aligned}
\tag{A.3}$$

The mean power in the $K_x - K_y$ grid, for the m^{th} antenna, is

$$P_{KG,m} = \sum_{k=-N_x/2}^{N_x/2-1} \sum_{l=-N_y/2}^{N_y/2-1} Em(k,l) ,
\tag{A.4}$$

and the mean power in the delay grid, for the m^{th} antenna, is

$$P_{DG,m} = \sum_{j=0}^{N_D-1} P_{mj} .
\tag{A.5}$$

These last two quantities are computed and output to ensure that the angular-delay grids contain most of the signal energy.

A.3 UNFORMATTED ACIRF OUTPUT FILES.

The overall file structure of the unformatted ACIRF output files which contain the impulse response function realizations is described in Table A.4.

The first record of an unformatted file is the 80 character identification that is input. The Fortran code that writes this record is shown in Table A.5.

The problem definition data record A contains a summary of the input data, and Record B contains a detailed definition of the realizations. The generating Fortran code is listed in Table A.6. A description of the important words in Record A is given in Table A.7. Because a common output file format is used by several channel simulation programs developed at Mission Research Corporation, ACIRF does not utilize all of the words in the record. Only the words that contain information relevant to the use of ACIRF realizations are listed in the table.

Table A.4. Structure of unformatted ACIRF output files.

Record	Description
1	Character identification record
2	Floating point record A (problem definition data)
3	Floating point record B (detailed problem definition data)
4	Record A
5	Floating point realization data record C_1
6	Record A (if necessary)
7	Floating point realization data record C_2 (if necessary)
•	•
•	•
•	•
2n	Record A (if necessary)
2n+2	Floating Point realization data record C_n (if necessary)

Table A.5. Fortran code that generates character identification record.

```

PARAMETER (NDENT=80)
CHARACTER IDENT*80
WRITE(IUNIT) NDENT,IDENT(1:NDENT)
    
```

Table A.6. Fortran code that generates floating point header records A and B.

```

PARAMETER (NDATA1=25,NDATA2=32)
COMMON/HEADER/RDATA1(NDATA1),RDATA2(NDATA2)
WRITE(IUNIT) NDATA1,(RDATA1(II),II=1,NDATA1)
WRITE(IUNIT) NDATA2,(RDATA2(II),II=1,NDATA2)
    
```

Table A.7. Description of header Record A.

RDATA1(1) = 2.0	ACIRF Realization
RDATA1(2) = KASE	Case Number
RDATA1(3) = FREQC	Carrier Frequency (Hz)
RDATA1(4) = TAUO	Decorrelation Time, τ_0 (sec)
RDATA1(5) = F0	Frequency Selective Bandwidth, f_0 (Hz)
RDATA1(6) = DLX	x Decorrelation Distance, ℓ_x (m)
RDATA1(7) = DLY	y Decorrelation Distance, ℓ_y (m)
RDATA1(9) = 1.0	Scintillation Index, S_4
RDATA1(13) = TDUR	Time Duration of Realization, ($N_T \Delta t$)
RDATA1(14) = NTIMES	Number of Time Samples, N_T
RDATA1(15) = DELTAT	Time Sample Size, Δt
RDATA1(16) = NO	Samples per Decorrelation Time, N_0
RDATA1(20) = NDELAY	Number of Delay Samples, N_D
RDATA1(22) = DELTAU	Delay Sample Size, $\Delta \tau$
RDATA1(23) = ISEED	Random Number Seed
RDATA1(25) = MAXBUF	Maximum Buffer Size

The ACIRF subroutines WRITER and READER which write and read the unformatted files are listed in Tables A.8 and A.9, respectively. The subroutine READER may be adapted to read the impulse response function into a link simulation. As currently written, READER outputs, through the call statement, an array containing the impulse response function $h(j\Delta\tau, n\Delta t)$ ($j = 1, \dots, N_D$) at a fixed time sample $n\Delta t$ ($n = 1, \dots, N_T$). Consecutive calls of READER produce consecutive time samples of the impulse response function.

The subroutine WRITER is called by ACIRF once each time step $n\Delta t$ ($n = 1, \dots, N_T$) and passed an array of the impulse response function $h(j\Delta\tau, n\Delta t,)$ ($j = 1, \dots, N_D$). WRITER buffers these arrays until the end of the realization is reached or until the number of impulse response function arrays equals the capacity of the buffer. The maximum number of arrays in buffer is equal to the largest integer which is less than or equal to $(\text{MAXBUF}/2)/N_{\text{DELAY}}$. The ACIRF parameter MAXBUF is the maximum number of real words in an unformatted file record. The current value of MAXBUF is 4096. Once the buffer is filled to capacity or the end of the realization is reached, WRITER writes the buffer into the file as a single record.

Table A.8. Listing of ACIRF subroutine WRITER.

```

SUBROUTINE WRITER(RESET,NDELAY,NTIMES,NFILE,IUNIT,H)
C
C***** VERSION 1.0 *** 25 NOV 1987 *****
C
C THIS SUBROUTINE WRITES A COMPLEX ARRAY INTO A FILE ON UNIT=IUNIT
C
C
C INPUTS:
C
C RESET = LOGICAL FLAG - INTIALIZATION IF RESET = .TRUE.
C H     = COMPLEX*8 ARRAY
C NDELAY = NUMBER OF DELAY SAMPLES IN IMPULSE RESPONSE FUNCTION
C NTIMES = NUMBER OF TIME SAMPLES IN IMPULSE RESPONSE FUNCTION
C NFILE  = FILE NUMBER
C IUNIT  = UNIT NUMBER OF FILE
C
C COMMON BLOCK INPUTS:
C
C RDATA1 = HEADER RECORD
C
C PARAMETERS:
C
C MAXBUF = MAXIMUM BUFFER SIZE (RECORD SIZE IN FILE = MAXBUF + 1)
C MTENNA = MAXIMUM NUMBER OF ANTENNAS (EQUAL TO MAXIMUM NUMBER OF FILES)
C NDATA1 = SIZE OF HEADER RECORD 1
C NDATA2 = SIZE OF HEADER RECORD 2
C
C*****
C
C     PARAMETER (MAXBUF=4096,MTENNA=8,NDATA1=25,NDATA2=32)
C     LOGICAL RESET
C     COMMON/HEADER/RDATA1(NDATA1),RDATA2(MTENNA,NDATA2)
C     COMPLEX H(NDELAY),BUFFER(MAXBUF/2,MTENNA)
C     DIMENSION NUMBER(MTENNA)
C
C***** IF RESET .EQ. TRUE THEN INITIALIZE
C

```

Table A.8. Listing of ACIRF subroutine WRITER (Concluded).

```

IF(RESET)THEN
  NTBUF = (MAXBUF/2)/NDELAY
  NCXWRD = NTBUF*NDELAY
  NRLWRD = 2*NCXWRD
  DO 10 NN=1,MTENNA
    NUMBER(NN) = 0
10  CONTINUE
  RESET = .FALSE.
  RETURN
END IF

C
C COUNT NUMBER OF CALLS - ONE PER TIME SAMPLE
C
  NUMBER(NFILE) = NUMBER(NFILE) + 1
  JOFFST = MOD((NUMBER(NFILE)-1)*NDELAY,NCXWRD)

C
C WRITE DELAY SAMPLES INTO BUFFER
C
  DO 20 JJ=1,NDELAY
    BUFFER(JOFFST+JJ,NFILE) = H(JJ)
20  CONTINUE
  IRTER = MOD(NUMBER(NFILE),NTBUF)

C
C WRITE BUFFER SAMPLES INTO FILE WHEN BUFFER IS FULL
C
  IF(IRTER .EQ. 0)THEN
    WRITE(IUNIT) NDATA1,(RDATA1(NN),NN=1,NDATA1)
    WRITE(IUNIT) NRLWRD,(BUFFER(KK,NFILE),KK=1,NCXWRD)
  END IF

C
C WRITE BUFFER SAMPLES INTO FILE WHEN AT END OF REALIZATION
C
  IF(NUMBER(NFILE) .EQ. NTIMES .AND. IRTER .NE. 0)THEN
    LFTCX = MOD(NTIMES,NTBUF)*NDELAY
    LFTRL = 2*LFTCX
    WRITE(IUNIT) NDATA1,(RDATA1(NN),NN=1,NDATA1)
    WRITE(IUNIT) LFTRL,(BUFFER(KK,NFILE),KK=1,LFTCX)
  END IF
  RETURN
END

```

Table A.9. Listing of ACIRF subroutine READER.

```

SUBROUTINE READER(RESET,NDELAY,NTIMES,NFILE,IUNIT,H)
C
C***** VERSION 1.1 *** 08 JUL 1988 *****
C
C THIS SUBROUTINE READS A COMPLEX ARRAY FROM A FILE ON UNIT=IUNIT
C ONE DELAY ARRAY IS READ FOR EACH CALL WITH RESET = .FALSE.
C THE INITIAL HEADER RECORDS ARE READ WITH RESET = .TRUE.
C
C INPUTS FROM ARGUMENT LIST:
C
C RESET = LOGICAL FLAG
C NDELAY = NUMBER OF DELAY SAMPLES IN IMPULSE RESPONSE FUNCTION
C         = DIMENSION OF H ARRAY
C NTIMES = NUMBER OF TIME SAMPLES IN IMPULSE RESPONSE FUNCTION
C NFILE  = FILE NUMBER (ONE PER ANTENNA)
C IUNIT  = UNIT OF FILE
C
C OUTPUTS TO ARGUMENT LIST:
C
C H      = IMPULSE RESPONSE FUNCTION ARRAY (DIMENSION NDELAY)
C
C COMMON BLOCK INPUTS:
C
C RDATA1 = HEADER RECORD
C
C PARAMETERS:
C
C MAXBUF = MAXIMUM BUFFER SIZE (RECORD SIZE IN FILE = MAXBUF + 1)
C MTENNA = MAXIMUM NUMBER OF ANTENNAS (EQUAL TO THE MAX NUMBER OF FILES)
C NDATA1 = SIZE OF HEADER RECORD 1
C NDATA2 = SIZE OF HEADER RECORD 2
C
C*****
C
C PARAMETER (MAXBUF=4096,MTENNA=8,NDATA1=25,NDATA2=32)
C COMMON/HEADER/RDATA1(NDATA1),RDATA2(MTENNA,NDATA2)
C COMPLEX H(NDELAY),BUFFER(MAXBUF/2,MTENNA)
C DIMENSION HEADER(NDATA1),NUMBER(MTENNA)
C LOGICAL RESET
C
C***** IF RESET = .TRUE. READ HEADER RECORDS AT BEGINNING OF FILE
C
C IF(RESET)THEN
C   REWIND IUNIT
C   READ(IUNIT)
C   READ(IUNIT) MDATA1,(HEADER(II),II=1,MINO(MDATA1,NDATA1))
C   READ(IUNIT)
C   MDATA1 = MINO(MDATA1,NDATA1)

```

Table A.9. Listing of ACIRF subroutine READER (Continued).

```

DO 10 NN=1,MDATA1
C
C FATAL ERROR IF HEADER RECORD DOES NOT AGREE WITH RDATA1
C IF(HEADER(NN) .NE. RDATA1(NN))THEN
WRITE(*,4000)NN,HEADER(NN),NN,RDATA1(NN)
4000 FORMAT(2X,'FATAL ERROR REREADING HEADER RECORD',/2X,
1 'WORD ',I2,' OF HEADER RECORD IS ',1PE12.5/2X,
2 'WORD ',I2,' OF HEADER RECORD SHOULD BE ',E12.5)
STOP
END IF
10 CONTINUE
NTBUF = (MAXBUF/2)/NDELAY
MAXCX = NTBUF*NDELAY
DO 20 NN=1,MTENNA
NUMBER(NN) = 0
20 CONTINUE
RESFT = .FALSE.
RETURN
END IF
NUMBER(NFILE) = NUMBER(NFILE) + 1
C
C COUNT NUMBER OF CALLS TO PROGRAM
C FATAL ERROR IF ATTEMPT TO READ BEYOND END of FILE
C
IF(NUMBER(NFILE) .GT. NTIMES)THEN
WRITE(*,4001)NUMBER(NFILE),NTIMES
4001 FORMAT(2X,'ATTEMPT TO READ BEYOND END of FILE',/2X,
1 'TIME INDEX = ',I10/2X,'MAX INDEX = ',I10)
STOP
END IF
C
C READ DATA INTO A BUFFER
C
IF(MOD(NUMBER(NFILE),NTBUF) .EQ. 1)THEN
READ(IUNIT) MDATA1,(HEADER(NN),NN=1,MINO(MDATA1,NDATA1))
READ(IUNIT) NRLWRD,
1 (BUFFER(KK,NFILE),KK=1,MINO(NRLWRD/2,MAXBUF/2))
MDATA1 = MINO(MDATA1,NDATA1)
DO 30 NN=1,MDATA1
C
C FATAL ERROR IF HEADER RECORD DOES NOT AGREE WITH RDATA1
C

```

Table A.9. Listing of ACIRF subroutine READER (Concluded).

```
        IF(HEADER(NN) .NE. RDATA1(NN))THEN
            WRITE(*,4000)NN,HEADER(NN),NN,RDATA1(NN)
            STOP
        END IF
30      CONTINUE
        END IF
C
C READ BUFFERED DATA INTO ARRAY
C
        JOFFST = MOD((NUMBER(NFILE)-1)*NDELAY,MAXCX)
        DO 40 JJ=1,NDELAY
            H(JJ) = BUFFER(JOFFST+JJ,NFILE)
40      CONTINUE
        RETURN
        END
```

The subroutine `READER` reverses this process. It first reads a record into a buffer, and then outputs a single impulse response function array from the buffer each time it is called. After $(\text{MAXBUF}/2)/\text{NDELAY}$ calls to `READER`, another record is read from the file into the buffer, and so on.

APPENDIX B

ACCURACY OF ANGULAR INTEGRATION TECHNIQUES

B.1 INTRODUCTION

The mean signal energy in a $K_x - K_y$ grid cell at the output of an antenna is

$$E(k, l) = \int_{(k-1/2)\Delta K_x}^{(k+1/2)\Delta K_x} \frac{dK_x}{2\pi} \int_{(l-1/2)\Delta K_y}^{(l+1/2)\Delta K_y} \frac{dK_y}{2\pi} G(K_x - K_{0x}, k_y - K_{0y}) S_k(K_x, K_y) \quad (\text{B.1})$$

This equation is quite general, but it requires that the energy in each angular bin be calculated and stored for each antenna. This latter requirement results in unacceptably large arrays. However, Equation B.1 can be approximated by assuming that the antenna beam profile varies slowly over the grid cells so $G(\vec{K} - \vec{K}_0)$ may be pulled out of the integral. There are several ways that this can be done. The purpose of this appendix is to calculate the accuracy of a few approximations to Equation B.1.

In order to limit the scope of this calculation, isotropic scattering and a uniformly weighted circular antenna will be assumed. Without loss of generality, it can then be assumed that the antenna is pointed away from the line of sight in the x direction, or equivalently, that the pointing azimuth is zero. For this case, the angular part of the GPSD is

$$S_K(K_x, K_y) = \pi \ell_0^2 \exp \left[-\frac{(K_x^2 + K_y^2) \ell_0^2}{4} \right], \quad (\text{B.2})$$

and the antenna beam profile is

$$G(K_x, K_y) = \exp \left[-\frac{\gamma(K_x^2 + K_y^2) \ell_0^2}{4} \right] \quad (\text{B.3})$$

where γ is proportional to the square of the ratio of the antenna diameter D to the decorrelation distance:

$$\gamma = \frac{4 \ln(2)}{(1.02899\pi)^2} \frac{D^2}{\ell_0^2} \quad . \quad (\text{B.4})$$

For this isotropic scattering and antenna case, the power at the output of the antenna reduces to

$$P_A = \frac{1}{1 + \gamma} \exp \left[-\frac{4 \ln(2) (\psi/\theta_0)^2}{1 + \gamma} \right] \quad (\text{B.5})$$

where ψ is the pointing angle and θ_0 is the beamwidth of the antenna. The antenna filtered decorrelation distance, which is the same in both the x and y directions is

$$\ell_A = \sqrt{1 + \gamma} \ell_0 \quad . \quad (\text{B.6})$$

The K_x angular grid size is then

$$\Delta K_x = \frac{4\pi}{N_x \ell_{Ax}} = \frac{4\pi}{N_x \sqrt{1 + \gamma} \ell_0} \quad . \quad (\text{B.7})$$

A similar expression holds for ΔK_y .

The exact expression for the received power will be compared to the total power in the grid,

$$P_G = \sum_{k=-N_x/2}^{N_x/2-1} \sum_{l=-N_y/2}^{N_y/2-1} E(k, l) \quad , \quad (\text{B.8})$$

to compute an error in the total power

$$P_E = \left| \frac{P_A - P_G}{P_A} \right| \quad (\text{B.9})$$

for each of the algorithms used to evaluate Equation B.1.

B.2 ALGORITHMS

The first approximation to the exact result is just Equation B.1. This expression will result in some error in the total power because of round-off errors in the summation of the contributions from each grid cell and because of the finite size of the angular grid. Additional error results when the beam is pointed near the edge of the grid so part of the beam is pointed out of the grid. The magnitude of this error will be apparent in the results of this analysis. With the assumptions of isotropic scattering and an isotropic Gaussian beam profile, the integrals indicated in Equation B.1 can be obtained in closed form with the result

$$E_1(k, l) = \frac{P_A}{4} \left\{ \operatorname{erfc} \left[\frac{(k-1/2)\Delta K_x \ell_0 \sqrt{1+\gamma}}{2} - \frac{\gamma K_0 \ell_0}{2\sqrt{1+\gamma}} \right] - \operatorname{erfc} \left[\frac{(k+1/2)\Delta K_x \ell_0 \sqrt{1+\gamma}}{2} - \frac{\gamma K_0 \ell_0}{2\sqrt{1+\gamma}} \right] \right\} \times \quad (\text{B.10})$$

$$\left\{ \operatorname{erfc} \left[\frac{(l-1/2)\Delta K_y \ell_0 \sqrt{1+\gamma}}{2} \right] - \operatorname{erfc} \left[\frac{(l+1/2)\Delta K_y \ell_0 \sqrt{1+\gamma}}{2} \right] \right\}$$

where $\operatorname{erfc}(\cdot)$ is the complementary error function and where

$$K_0 \ell_0 = (1.02899\pi) \frac{\psi \ell_0}{\theta_0 D} \quad (\text{B.11})$$

The second approximation, and the one that is used in ACIRF, is obtained by assuming that the antenna beam profile is constant over an angular grid cell and can therefore be pulled out of the integral. The result is the product of the antenna beam profile times a term that is equal to the incident energy in a grid cell:

$$E_2(k, l) = G(K_x - K_{0x}, K_y - K_{0y}) E_I(k, l) \quad (\text{B.12})$$

where the incident energy is

$$E_I(k, l) = \int_{(k-1/2)\Delta K_x}^{(k+1/2)\Delta K_x} \frac{dK_x}{2\pi} \int_{(l-1/2)\Delta K_y}^{(l+1/2)\Delta K_y} \frac{dK_y}{2\pi} S_K(K_x, K_y) \quad (\text{B.13})$$

The indicated integrals can again be expressed in terms of error functions:

$$E_I(k, l) = \frac{1}{2} \left\{ \operatorname{erfc} \left[\frac{(k - 1/2)\Delta K_x \ell_0}{2} \right] - \operatorname{erfc} \left[\frac{(k + 1/2)\Delta K_x \ell_0}{2} \right] \right\} \times \\ \frac{1}{2} \left\{ \operatorname{erfc} \left[\frac{(l - 1/2)\Delta K_y \ell_0}{2} \right] - \operatorname{erfc} \left[\frac{(l + 1/2)\Delta K_y \ell_0}{2} \right] \right\} \quad (\text{B.14})$$

The advantage of this approximation is that the error function terms depend only on the environment so they can be done once and used for all antennas thereby reducing the required processing time and array sizes.

A third approximation to Equation B.1 is similar to the previous approximation. Rather than using the antenna gain at the center of each angular grid cell, the gain averaged over the grid cell is used:

$$E_3(k, l) = E_I(k, l) \frac{1}{\Delta K_x \Delta K_y} \int_{(k-1/2)\Delta K_x}^{(k+1/2)\Delta K_x} dK_x \int_{(l-1/2)\Delta K_y}^{(l+1/2)\Delta K_y} dK_y G(K_x - K_{0x}, K_y - K_{0y}) \quad (\text{B.15})$$

Writing the indicated integrals in terms of error functions gives the result:

$$E_3(k, l) = E_I(k, l) \frac{\pi}{\Delta K_x \Delta K_y \gamma \ell_0^2} \times \\ \left\{ \operatorname{erfc} \left[\frac{\sqrt{\gamma} |(k - 1/2)\Delta K_x - K_0| \ell_0}{2} \right] - \operatorname{erfc} \left[\frac{\sqrt{\gamma} |(k + 1/2)\Delta K_x - K_0| \ell_0}{2} \right] \right\} \times \\ \left\{ \operatorname{erfc} \left[\frac{\sqrt{\gamma} (l - 1/2)\Delta K_y \ell_0}{2} \right] - \operatorname{erfc} \left[\frac{\sqrt{\gamma} (l + 1/2)\Delta K_y \ell_0}{2} \right] \right\} \quad (\text{B.16})$$

Finally, a simple way to eliminate the problem created by Equation B.1 is to do away with the integral. This zeroth order approximation is

$$E_4(k, l) = \frac{\Delta K_x \Delta K_y}{4\pi^2} G(k\Delta K_x - K_{0x}, l\Delta K_y - K_{0y}) S_K(k\Delta K_x, l\Delta K_y) \quad (\text{B.17})$$

B.3 RESULTS

The relative error (Equation B.9) of the four algorithms is calculated for a range of the ratio of the decorrelation distance to the antenna diameter. The scattering loss of the antenna for this range of ℓ_0/D is shown in Figure 2.5 for pointing angles of 0, $\theta_0/2$, and θ_0 . Figures B.1, B.2 and B.3 show the relative errors of the four algorithms for the same set of pointing angles. For these calculations, a 32×32 angular grid is used. This is the smallest angular grid size used in ACIRF.

When the pointing angle is zero, algorithm 1 (solid line) has a relatively constant error of about 2×10^{-5} . This error is attributed to round-off errors that result in performing the sum of $E(k, l)$ over all grid cells. Both algorithms 2 (dashed line) and 3 (dotted line) for this case have peak errors of about 10^{-3} which occur when the angular spread of the incident energy is about equal to the antenna beamwidth (i.e. ℓ_0 is approximately equal to D). Algorithm 4 (dash-dot-dash line) has a maximum relative error for large values of ℓ_0/D of about 2.5, which is unacceptably large.

As the pointing angle increases, the maximum error of algorithm 1 increases due to the fact that part of the beam is pointing out of the angular grid. However, even when the pointing angle is equal to a beamwidth, this error is less than 2 percent, and it is less than 0.1 percent when the pointing angle is one-half of a beamwidth. Algorithms 2 and 3 generally have errors which are close to that of algorithm 1. The maximum error of these algorithms is less than 2.5×10^{-3} when the pointing angle is $\theta_0/2$. When the pointing angle is equal to a beamwidth, the sign of the errors of algorithms 2 and 3 change over the range of ℓ_0/D resulting in errors that are smaller in magnitude than that of algorithm 1.

Algorithm 2 generally has a slightly smaller error than algorithm 3 over the ranges of ℓ_0/D and pointing angles considered in this analysis. Algorithm 2 is also easier to implement than is algorithm 3. Based on these results, the second algorithm is used in ACIRF.

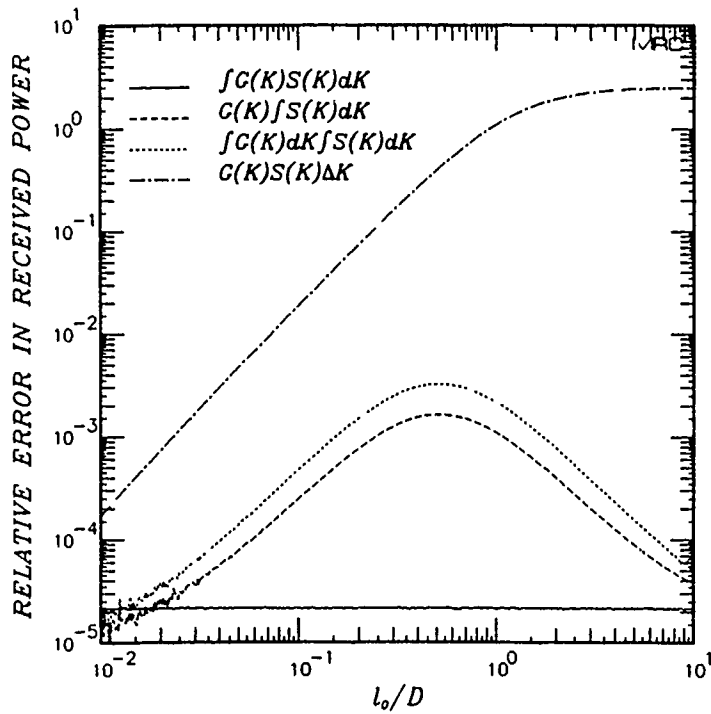


Figure B.1. Relative error for pointing angle of 0.

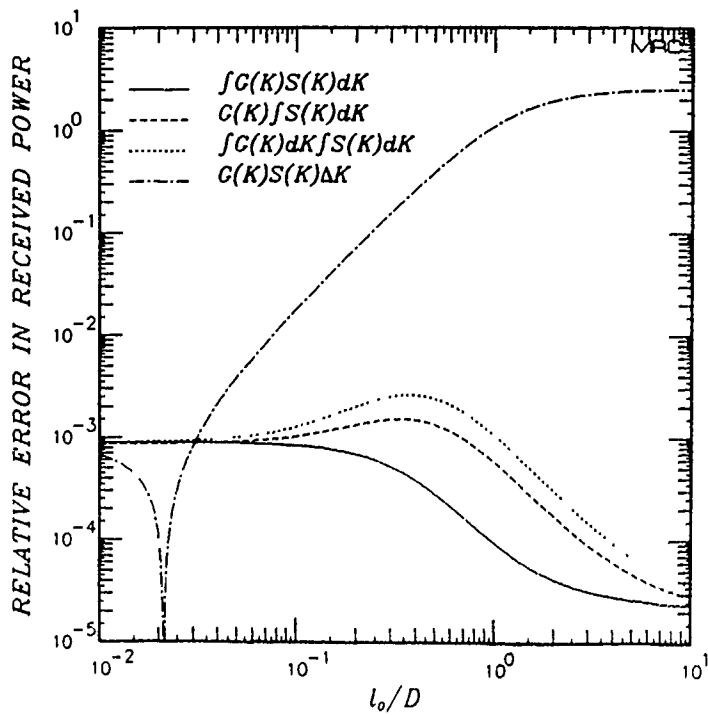


Figure B.2. Relative error for pointing angle of $\theta_0/2$.

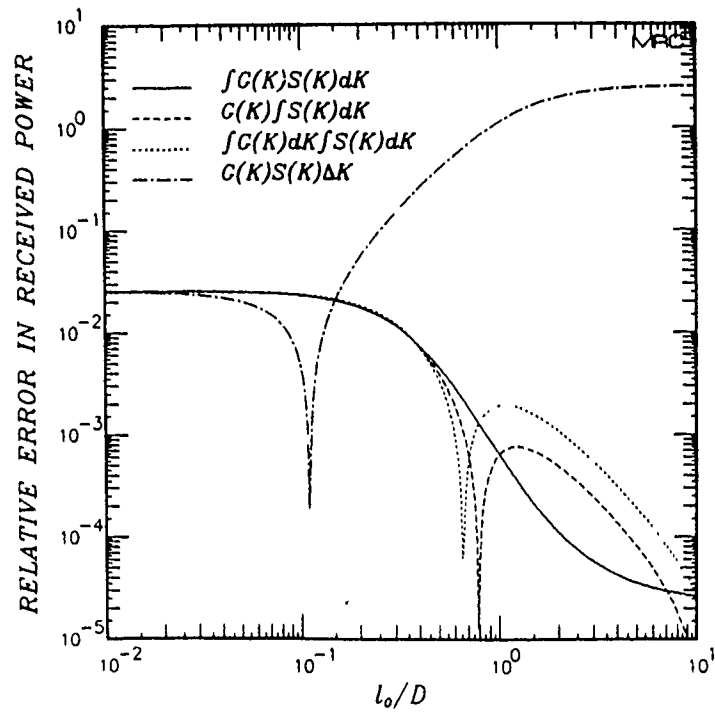


Figure B.3. Relative error for pointing angle of θ_0 .

DISTRIBUTION LIST

DNA-TR-88-175

DEPARTMENT OF DEFENSE

(US NUCLEAR COM & CENTRAL SYST SUP STAFF)
ATTN: SAB H SEQUINE

ASSISTANT TO THE SECRETARY OF DEFENSE
ATOMIC ENERGY
ATTN: EXECUTIVE ASSISTANT

DEFENSE ADVANCED RSCH PROJ AGENCY
ATTN: DR MANSFIELD
ATTN: GSD R ALEWINE

DEFENSE COMMUNICATIONS AGENCY
ATTN: A320
ATTN: J DIETZ

DEFENSE COMMUNICATIONS ENGINEER CENTER
ATTN: CODE R410

DEFENSE INTELLIGENCE AGENCY
ATTN: DC-6
ATTN: DIR
ATTN: DT-1B
ATTN: RTS-2B
ATTN: VP-TPO

DEFENSE NUCLEAR AGENCY
ATTN: DFSP G ULLRICH
ATTN: NANF
ATTN: NASF
ATTN: OPNA
ATTN: PRPD R YOHO
3 CYS ATTN: RAAE
ATTN: RAAE A MARDIGUIAN
ATTN: RAAE G ULLRICH
ATTN: RAAE K SCHWARTZ
ATTN: RAAE L SCHROCK
ATTN: RAAE M CRAWFORD
ATTN: RAAE P FLEMING
ATTN: RAAE S BERGGREN
ATTN: RAAE

4 CYS ATTN: TITL

DEFENSE NUCLEAR AGENCY
ATTN: TDNM
2 CYS ATTN: TDTT W SUMMA

DEFENSE TECHNICAL INFORMATION CENTER
2 CYS ATTN: DTIC/FDAB

JOINT DATA SYSTEM SUPPORT CTR
ATTN: C-312 R MASON

JOINT STRAT TGT PLANNING STAFF
ATTN: JK (ATTN: DNA REP)
ATTN: JKCS, STUKMILLER
ATTN: JLWT (THREAT ANALYSIS)
ATTN: JPEM
ATTN: JPSS

NATIONAL SECURITY AGENCY
ATTN: B432 C GOEDEKE

STRATEGIC AND THEATER NUCLEAR FORCES
ATTN: DR E SEVIN
ATTN: DR SCHNEITER
ATTN: LC R DAWSON

STRATEGIC DEFENSE INITIATIVE ORGANIZATION
ATTN: C GIESE
ATTN: K OBRIEN
ATTN: KE
ATTN: S/AA COL GUIBERSON
ATTN: S/AA W SEIBERLING
ATTN: SLKT
ATTN: SN
ATTN: T/SK COL R ROSS

THE JOINT STAFF
ATTN: J6

DEPARTMENT OF THE ARMY

ARMY LOGISTICS MANAGEMENT CTR
ATTN: DLSIE

DEP CH OF STAFF FOR OPS & PLANS
ATTN: DAMO-RQC C2 DIV

HARRY DIAMOND LABORATORIES
ATTN: SLCIS-IM-TL

U S ARMY ATMOSPHERIC SCIENCES LAB
ATTN: DR F NILES
ATTN: SLCAS-AE-E
ATTN: SLCAS-AR DR H HOLT

U S ARMY COMMUNICATIONS R&D COMMAND
ATTN: AMSEL-RD-ESA

U S ARMY FOREIGN SCIENCE & TECH CTR
ATTN: DRXST-SD

U S ARMY MISSILE COMMAND/AMSMI-RD-CS-R
ATTN: AMSMI-RD-CS-R

U S ARMY NUCLEAR & CHEMICAL AGENCY
ATTN: MONA-NU

U S ARMY NUCLEAR EFFECTS LABORATORY
ATTN: ATAA-PL
ATTN: ATAA-TDC
ATTN: ATRC-WCC

U S ARMY STRATEGIC DEFENSE CMD
ATTN: BMDSC-HI M POPE
ATTN: CSSD-H-TT M POPE
ATTN: DASD-H-SA R BRADSHAW
ATTN: DASD-H-SA/R SMITH
ATTN: DASD-H-SAV

U S ARMY STRATEGIC DEFENSE COMMAND
ATTN: ATC-O W DAVIES
ATTN: BMDATC-R W DICKERSON

U S ARMY WHITE SANDS MISSILE RANGE
ATTN: STEWS-TE-N K CUMMINGS

DNA-TR-88-175 (DL CONTINUED)

USA SURVIVABILITY MANAGEMENT OFFICE
ATTN: SLCSM-SE J BRAND

DEPARTMENT OF THE NAVY

COMMAND & CONTROL PROGRAMS
ATTN: OP 941

JOINT CRUISE MISSILES PROJECT OFC (PM-3)
ATTN: JCMG-707

NAVAL AIR SYSTEMS COMMAND
ATTN: PMA 271

NAVAL ELECTRONICS LNDRG ACTVY, PACIFIC
ATTN: CODE 250 D OBRYHIM

NAVAL OCEAN SYSTEMS CENTER
ATTN: CODE 542, J FERGUSON

NAVAL RESEARCH LABORATORY
ATTN: CODE 2000 J BROWN
ATTN: CODE 2627

2 CYS ATTN: CODE 4100 H GUNSKY
ATTN: CODE 4121.8 H HECKATHORN
ATTN: CODE 4183
ATTN: CODE 4700 S OSSAKOW
ATTN: CODE 4701
ATTN: CODE 4720 J DAVIS
ATTN: CODE 4750 P RODRIGUEZ
ATTN: CODE 4780 B RIPIN
ATTN: CODE 4780 DR P BERNHARDT
ATTN: CODE 4780 J HUBA
ATTN: CODE 5300
ATTN: CODE 8344 M KAPLAN

NAVAL SURFACE WARFARE CENTER
ATTN: CODE H-21

NAVAL TECHNICAL INTELLIGENCE CTR
ATTN: DA44

NAVAL UNDERWATER SYSTEMS CENTER
ATTN: CODE 3411, J KATAN

OFC OF THE DEPUTY CHIEF OF NAVAL OPS
ATTN: OP 554
ATTN: OP 941D
ATTN: OP 981N

OFFICE OF NAVAL RESEARCH
ATTN: 1132SM A TUCKER

SPACE & NAVAL WARFARE SYSTEMS CMD
ATTN: CODE 3101 T HUGHES
ATTN: PD 50TD
ATTN: PD50TD1 G BRUNHART
ATTN: PME 106-4 S KEARNEY
ATTN: PME-106 F W DIEDERICH

THEATER NUCLEAR WARFARE PROGRAM OFC
ATTN: PMS-42331F D SMITH

DEPARTMENT OF THE AIR FORCE

AIR FORCE CTR FOR STUDIES & ANALYSIS
ATTN: AFCSA/SAMI R GRIFFIN
ATTN: AFCSA/SASC

AIR FORCE ELECTRONIC WARFARE CENTER
ATTN: LT M MCNEELY

AIR FORCE SPACE SYSTEMS DIVISION
ATTN: CNSC T ABOUSHI
ATTN: YA
2 CYS ATTN: YN

AIR FORCE TECHNICAL APPLICATIONS CTR
ATTN: TN

AIR UNIVERSITY LIBRARY
ATTN: AUL-LSE

BALLISTIC SYSTEMS DIVISION
ATTN: ENSE
ATTN: PK

HQ AWS, DET 3 CSTC/WE
ATTN: WE

SECRETARY OF AF/AQQS
ATTN: AF/RDQI

STRATEGIC AIR COMMAND/XRFS
ATTN: XRFS

WEAPONS LABORATORY
ATTN: NTCA
ATTN: NTN
ATTN: SUL

DEPARTMENT OF ENERGY

EG&G, INC
ATTN: D WRIGHT

LAWRENCE LIVERMORE NATIONAL LAB
ATTN: L-31 R HAGER
ATTN: L-97 T DONICH

LOS ALAMOS NATIONAL LABORATORY
ATTN: D SAPPENFIELD
ATTN: D SIMONS
ATTN: D WINSKE
ATTN: F670 MS J MALIK
ATTN: J WOLCOTT
ATTN: MS J ZINN
ATTN: R W WHITAKER ESS-5
ATTN: T KUNKLE, ESS-5

SANDIA NATIONAL LABORATORIES
ATTN: D HARTLEY 8300

SANDIA NATIONAL LABORATORIES
ATTN: A D THORNBROUGH 400
ATTN: C. S. WILLIAMS 2344
ATTN: CODE 9014 R BACKSTROM
ATTN: D DAHLGREN 6440
ATTN: ORG 1231 T P WRIGHT
ATTN: ORG 7112 C MEHL
ATTN: ORG 9114 W D BROWN
ATTN: SPACE PROJECT DIV
ATTN: TECH LIB 3141

OTHER GOVERNMENT

CENTRAL INTELLIGENCE AGENCY
ATTN: OSWR/NED
ATTN: OSWR/SSD FOR L BERG

DEPARTMENT OF COMMERCE
ATTN: E MORRISON
ATTN: G REEVE
ATTN: J HOFFMEYER
ATTN: W UTLAUT

U S DEPARTMENT OF STATE
ATTN: PM/TMP

DEPARTMENT OF DEFENSE CONTRACTORS

AEROSPACE CORP
ATTN: A LIGHTY
ATTN: A MORSE
ATTN: B P PURCELL
ATTN: C CREWS
ATTN: C RICE
ATTN: G LIGHT
ATTN: I GARFUNKEL
ATTN: J KLUCK
ATTN: M ROLENZ

ANALYTICAL SYSTEMS ENGINEERING CORP
ATTN: SECURITY

ATLANTIC RESEARCH SERVICES CORP
ATTN: R MCMILLAN

ATMOSPHERIC AND ENVIRONMENTAL RESEARCH INC
ATTN: M KO

AUSTIN RESEARCH ASSOCIATES
ATTN: J THOMPSON

AUTOMETRIC INCORPORATED
ATTN: C LUCAS

BDM INTERNATIONAL INC
ATTN: L JACOBS

BERKELEY RSCH ASSOCIATES, INC
ATTN: C PRETTIE
ATTN: J WORKMAN
ATTN: S BRECHT

BOEING CO
ATTN: G HALL

CALIFORNIA RESEARCH & TECHNOLOGY, INC
ATTN: M ROSENBLATT

CHARLES STARK DRAPER LAB, INC
ATTN: A TETEWSKI

COMMUNICATIONS SATELLITE CORP
ATTN: G HYDE

CORNELL UNIVERSITY
ATTN: D FARLEY JR
ATTN: M KELLY

ELECTROSPACE SYSTEMS, INC
ATTN: P PHILLIPS

EOS TECHNOLOGIES, INC
ATTN: B GABBARD
ATTN: W LELEVIER

GENERAL ELECTRIC CO
ATTN: R EDSALL

GENERAL RESEARCH CORP INC
ATTN: J EOLL

GEO CENTERS, INC
ATTN: E MARRAM

GRUMMAN AEROSPACE CORP
ATTN: J DIGLIO

GTE GOVERNMENT SYSTEMS CORPORATION
ATTN: W I THOMPSON, III

HARRIS CORPORATION
ATTN: E KNICK

HSS, INC
ATTN: D HANSEN

INFORMATION SCIENCE, INC
ATTN: W DUDZIAK

INSTITUTE FOR DEFENSE ANALYSES
ATTN: E BAUER
ATTN: H WOLFHARD

J S LEE ASSOCIATES INC
ATTN: DR J LEE

JAYCOR
ATTN: J SPERLING

JOHNS HOPKINS UNIVERSITY
ATTN: C MENG
ATTN: J D PHILLIPS
ATTN: R STOKES
ATTN: T EVANS

KAMAN SCIENCES CORP
ATTN: E CONRAD
ATTN: G DITTBERNER

KAMAN SCIENCES CORPORATION
ATTN: B GAMBILL
ATTN: DASIAC
ATTN: R RUTHERFORD

KAMAN SCIENCES CORPORATION
ATTN: DASIAC

LOCKHEED MISSILES & SPACE CO, INC
ATTN: J HENLEY
ATTN: J KUMER
ATTN: R SEARS

LOCKHEED MISSILES & SPACE CO, INC
ATTN: D KREJCI

LTV AEROSPACE & DEFENSE COMPANY
2 CYS ATTN: LIBRARY

DNA-TR-88-175 (DL CONTINUED)

M I T LINCOLN LAB

ATTN: D TOWLE L-230
ATTN: I KUPIEC L-100
ATTN: M LEE G91

MARTIN MARIETTA DENVER AEROSPACE

ATTN: H VON STRUVE III
ATTN: 50018 J BENNETT

MAXIM TECHNOLOGIES, INC

ATTN: B RIDGEWAY
ATTN: J SO

MCDONNELL DOUGLAS CORP

ATTN: T CRANOR

MCDONNELL DOUGLAS CORPORATION

ATTN: J GROSSMAN
ATTN: R HALPRIN

METATECH CORPORATION

ATTN: R SCHAEFER
ATTN: W RADASKY

METEOR COMMUNICATIONS CORP

ATTN: R LEADER

MISSION RESEARCH CORP

ATTN: J KENNEALY
ATTN: R ARMSTRONG
ATTN: R LARKIN
ATTN: S BELANGER
ATTN: W WHITE

MISSION RESEARCH CORP

ATTN: B R MILNER
ATTN: C LONGMIRE
ATTN: D ARCHER
ATTN: D KNEPP
ATTN: D LANDMAN
ATTN: F FAJEN
ATTN: F GUIGLIANO
ATTN: G MCCARTOR
ATTN: K COSNER
ATTN: M FIRESTONE
ATTN: R BIGONI
ATTN: R BOGUSCH

2 CYS

ATTN: R DANA
ATTN: R HENDRICK
ATTN: R KILB
ATTN: S GUTSCHE
ATTN: TECH INFO CENTER
ATTN: TECH LIBRARY

MITRE CORPORATION

ATTN: D RAMPTON, PH.D
ATTN: M R DRESP

MITRE CORPORATION

ATTN: J WHEELER
ATTN: M HORROCKS
ATTN: R C PESCI
ATTN: W FOSTER

NORTHWEST RESEARCH ASSOC, INC

ATTN: E FREMOUW

PACIFIC-SIERRA RESEARCH CORP

ATTN: E FIELD JR
ATTN: F THOMAS
ATTN: H BRODE

PHOTOMETRICS, INC

ATTN: I L KOFSKY

PHOTON RESEARCH ASSOCIATES

ATTN: D BURWELL
ATTN: O LEWIS

PHYSICAL RESEARCH INC

ATTN: W. SHIH

PHYSICAL RESEARCH INC

ATTN: H FITZ
ATTN: P LUNN

PHYSICAL RESEARCH, INC

ATTN: R DELIBERIS
ATTN: T STEPHENS

PHYSICAL RESEARCH, INC

ATTN: J DEVORE
ATTN: J THOMPSON
ATTN: W SCHLUETER

R & D ASSOCIATES

ATTN: C GREIFINGER
ATTN: F GILMORE
ATTN: G HOYT
ATTN: M GANTSWEG

R & D ASSOCIATES

ATTN: J WALTON

RAND CORP

ATTN: C CRAIN
ATTN: E BEDROZIAN

RAND CORP

ATTN: B BENNETT

RJO ENTERPRISES/POET FAC

ATTN: A ALEXANDER
ATTN: W BURNS

S-CUBED

ATTN: C NEEDHAM
ATTN: T CARNEY

SCIENCE APPLICATIONS INTL CORP

ATTN: S ROSENWEIG

SCIENCE APPLICATIONS INTL CORP

ATTN: C SMITH
ATTN: D HAMLIN
ATTN: D SACHS
ATTN: E STRAKER
ATTN: L LINSON

SCIENCE APPLICATIONS INTL CORP

ATTN: J COCKAYNE

SCIENCE APPLICATIONS INTL CORP

ATTN: D TELAGE
ATTN: M CROSS

SRI INTERNATIONAL

ATTN: D MCDANIEL
ATTN: J DEPP
ATTN: R LEONARD
ATTN: W CHESNUT
ATTN: W JAYE

STEWART RADIANCE LABORATORY

ATTN: R HUPPI

TELECOMMUNICATION SCIENCE ASSOCIATES

ATTN: R BUCKNER

TELEDYNE BROWN ENGINEERING

ATTN: J WOLFSBERGER, JR
ATTN: N PASSINO

TOYON RESEARCH CORP

ATTN: J ISE

TRW INC

ATTN: DR D GRYBOS
ATTN: R PLEBUCH
ATTN: R5/220 H CULVER

TRW SPACE & DEFENSE SYSTEMS

ATTN: D M LAYTON

USER SYSTEMS, INC

ATTN: S W MCCANDLESS, JR

UTAH STATE UNIVERSITY

ATTN: K BAKER
ATTN: L JENSEN, ELEC ENG DEPT

VISIDYNE, INC

ATTN: J CARPENTER

FOREIGN

FOA 2

ATTN: B SJOHOLM

FOA 3

ATTN: T KARLSSON